Received: 30 December 2021 | Revised: 13 February 2022 | Accepted: 22 February 2022

DOI: 10.1111/pce.14316

ORIGINAL ARTICLE

Plant, Cell & Environment | WILEY

A novel calmodulin-interacting Domain of Unknown Function 506 protein represses root hair elongation in *Arabidopsis*

Sheng Ying | **Wolf-Rüdiger Scheible**

Noble Research Institute LLC, Ardmore, Oklahoma, USA

Correspondence
Sheng Ying, Department of Biochemistry and Molecular Biology, Michigan State University, East Lansing, MI 48823, USA.
Email: yingshen@msu.edu

Funding information
Noble Research Institute

Abstract

Domain of Unknown Function 506 proteins are ubiquitous in plants. The phosphorus (P) stress-inducible *REPRESSOR OF EXCESSIVE ROOT HAIR GROWTH1* (*AtRXR1*) gene encodes the first characterized DUF506. AtRXR1 inhibits root hair elongation by interacting with RabD2c GTPase. However, functions of other P-responsive *DUF506* genes are still missing. Here, we selected two additional P-inducible *DUF506* genes for further investigation. The expression of both genes was induced by auxin. Under P-stress, *At3g07350* gene expressed ubiquitously in seedlings, whereas *At1g62420* (*AtRXR3*) expression was strongest in roots. *AtRXR3* overexpressors and knockouts had shorter and longer root hairs, respectively. A functional AtRXR3-green fluorescent protein fusion localized to root epidermal cells. Chromatin immunoprecipitation and quantitative reverse-transcriptase-polymerase chain reaction revealed that *AtRXR3* was transcriptionally activated by RSL4. Bimolecular fluorescence complementation and calmodulin (CaM)-binding assays showed that AtRXR3 interacted with CaM in the presence of Ca^{2+}. Moreover, cytosolic Ca^{2+} ($[Ca^{2+}]_{cyt}$) oscillations in root hairs of *rxr3* mutants exhibited elevated frequencies and dampened amplitudes compared to those of wild type. Thus, AtRXR3 is another DUF506 protein that attenuates P-limitation-induced root hair growth through mechanisms that involve RSL4 and interaction with CaM to modulate tip-focused $[Ca^{2+}]_{cyt}$ oscillations.

KEYWORDS
calcium oscillation, phosphorus stress, root hair growth, RSL4

1 | INTRODUCTION

Phosphorus (P) is a structural component of nucleic acids, membrane phospholipids and energy metabolites. As such, P is essential for all life on earth. Plants assimilate P as inorganic phosphate (Pi) from the soil. However, the concentration of Pi in many unfertilized soils is low and therefore limiting for plant growth (Hammond et al., 2004; Raghothama, 1999). Plants employ various strategies to improve the acquisition, remobilization and efficient use of Pi when P is limited. The strategies include altering root morphology and secreting phosphatases and nucleases to mobilize or release Pi from soil insoluble organic sources (Lynch, 2011; Plaxton & Tran, 2011; Svistoonoff et al., 2007; Williamson et al., 2001). Increasing the density and length of root hairs (RHs) is one morphological response

of roots to low P. RHs account for up to 70% of the total root surface area in many plant species. The increase in root surface area due to RHs facilitates the absorbance of soil Pi (Bates & Lynch, 2001; Bucher, 2007; Crombez et al., 2019; Lynch, 2019; Ma et al., 2003). Moreover, longer RHs improve root penetration in hard and dry soils (Choi & Cho, 2019; Haling et al., 2013), enhance plant tolerance to drought stress (Marin et al., 2020; Zhang et al., 2020) and enable roots to interact more efficiently with beneficial microbes (Brown et al., 2013).

RHs develop from specialized root epidermal cells called trichoblasts. In *Arabidopsis*, trichoblasts are located between two underlying cortical cells (Grierson et al., 2014). Among the many genes that function in RH formation, *ROOT HAIR DEFECTIVE6* (*RHD6*), which encodes a bHLH transcription factor (TF), stands out (Masucci & Schiefelbein, 1994). RHD6, along with RHD6-LIKE2 (RSL2) and RHD6-LIKE4 (RSL4) directly bind to promoter RH elements (RHEs, $TN_6CA[CT]G[TA]$) of various RH-specific (RHS) genes. Binding of these bHLH TFs to RHEs modulate the expression of RHS genes and consequently RH elongation (Bhosale et al., 2018; Datta et al., 2015; Hwang et al., 2017; Kim & Dolan, 2016; Kim et al., 2017; Vijayakumar et al., 2016; Yi et al., 2010).

Phytohormones and other signalling factors, such as reactive oxygen species (ROS), calcium ions (Ca^{2+}) and the short peptide RAPID ALKALINIZATION FACTOR1 (AtRALF1), modulate RH development (Abarca et al., 2021; Feng et al., 2017; Foreman et al., 2003; Han et al., 2020; Kapulnik et al., 2011; Mangano et al., 2017, 2018; Pitts et al., 1998; Tian et al., 2020; Vissenberg et al., 2020; Wang et al., 2017; Zhu et al., 2020). Two models explain the mechanisms of RH elongation when exposed to low external P (Bhosale et al., 2018; Song et al., 2016). One model proposes that under P-deficiency, elevated endogenous auxin activates auxin influx carrier (AUX1)-mediated auxin transport and induces *auxin response factor19* (*ARF19*) expression. The activation of auxin transport and signalling then stimulates the expression of *RSL2* and *RSL4* to enhance RH elongation. The second model postulates that the ethylene-activated TF ETHYLENE-INSENSITIVE3 (EIN3) regulates P-limitation-induced RH growth by interacting with RHD6 or activating the expression of RSL4 target genes (Feng et al., 2017; Song et al., 2016).

P starvation significantly affects the cytosolic Ca^{2+} ($[Ca^{2+}]_{cyt}$) signature of *Arabidopsis* roots (Matthus et al., 2019). $[Ca^{2+}]_{cyt}$ signatures are decoded by the Ca^{2+}-binding protein, calmodulin (CaM) and related proteins collectively called CaM-like proteins (CMLs). In *Arabidopsis*, seven genes encode for CaMs and another 50 encode CMLs (Zielinski, 1998). CaMs associate with other enzymatic effectors such as cyclic nucleotide-gated channels (CNGCs) to facilitate their regulatory functions (Brost et al., 2019). The NADPH oxidase, ROOT HAIR DEFECTIVE2, triggers the accumulation of ROS, which subsequently specifies the frequency and amplitude of $[Ca^{2+}]_{cyt}$ oscillations, and steepness of $[Ca^{2+}]_{cyt}$ gradients at the RH tip through the activation of CNGCs (Foreman et al., 2003; Tian et al., 2020). Plasma membrane-localized CNGC14 mediates Ca^{2+} influx into elongating RHs (Zhang et al., 2017). Moreover, CaM7 interacts with CNGC14 in *Arabidopsis* to inhibit RH growth (Zeb et al., 2020). Although there is accumulating evidence for the involvement of CaM and $[Ca^{2+}]_{cyt}$ in RH elongation, their role in modulating P-starvation-induced RH growth is unknown.

The Domain of Unknown Function 506 (DUF506) gene family is omnipresent in many plant species (Ying et al., 2022). The *Arabidopsis* genome has 13 *DUF506* genes. The proteins encoded by these genes have three conserved domains, which are concentrated in the C-terminus. On the other hand, the N-terminus of DUF506 is highly diverse (Ying, 2021). The only characterized *DUF506* gene so far is *At3g25240* (*AtRXR1*). *AtRXR1* is strongly induced by P-stress in a PHR1/PHL1-dependent manner. The PHR1/PHL1-AtRXR1 represses RH elongation based on overexpression and mutant studies. Similar to *Arabidopsis*, overexpressing the *Brachypodium RXR1* orthologue (*Bdi2g58590*) in *Brachypodium distachyon* leads to short RH (Ying et al., 2022).

The effect of RXR1 on P-limitation-mediated RH growth prompted us to study other *Arabidopsis DUF506* genes, particularly those whose expression was induced by low P. One *Arabidopsis DUF506* gene (*At1g62420*, hereafter referred to as *AtRXR3*) was investigated in more detail. Our results reveal that, like AtRXR1, AtRXR3 is a repressor of RH elongation growth. However, the mechanism by which AtRXR3 represses RH growth differs from that of AtRXR1. While AtRXR1 represses RH growth via a small GTPase, AtRXR3 does so through RSL4 and its interaction with various cytosolic CaMs.

2 | MATERIALS AND METHODS

2.1 | Plant material, growth and treatment

Arabidopsis thaliana (ecotype Col-0) seeds were sterilized and placed on a half-strength Murashige and Skoog (1/2MS) solid medium according to (Ying et al., 2022). Petri dishes were stratified for 3 days at 4°C in the dark before transfer to a growth chamber (120 μmol^{-2} s^{-1} light intensity, 22°C/20°C, 16 h light cycle and 8 h dark cycle). For phosphate-deprived (−P) treatment, experiments were performed as described previously (Morcuende et al., 2007). Briefly, *Arabidopsis* seedlings were germinated and grown in 1/2MS liquid medium and then transferred into P-deficient liquid culture on Day 7. Shoot and root tissues were harvested on Day 9 or as indicated in Section 4, frozen in liquid N_2 and stored in −80°C freezer. The *rxr3-1* (Salk_016908), *rxr3-2* (Salk_078603), *cam7* (CS873256) and *arf7 arf19* (CS24629) T-DNA insertion mutant lines were obtained from Arabidopsis Biological Resource Center (ABRC). The *rsl4* mutant was kindly provided by Dr. Elison Blancaflor (Noble Research Institute). Homozygous mutant plants were identified or validated according to the SiGnAL database protocol (http://signal.salk.edu/).

2.2 | Quantitative reverse transcription-PCR (qRT-PCR)

Total RNA was extracted using RNeasy® plant mini kit (Qiagen) and genomic DNA was removed using Turbo DNA-free™ kit (Invitrogen)

following the manufacturer's instructions. RNA (1 μg) was converted into cDNA using SuperScript™ III Reverse Transcriptase (Invitrogen) according to the manufacturer's instruction. Quantitative PCR was performed using QuantStudio™ 7 Flex Real-Time PCR System (Invitrogen) and KiCqStart® SYBR® Green qPCR ReadyMix™ (Millipore Sigma). The qRT-PCR reaction procedures were conducted as described previously (Ying et al., 2022). The *Arabidopsis GAPDH* (*At1g13440*) gene was used as an internal control (Czechowski et al., 2005). All the experiments were repeated at least three times using cDNAs prepared from two different biological replicates with representative results shown in the figures. Sequences of primers used in the study are listed in Table S2.

2.3 | Measurement of RH length

Seedlings were germinated vertically for 3 days on 1/2MS solid medium containing 0.4% Gelzan™ CM (Millipore Sigma) and then transferred to plates containing either 0 (P-deficient) or 675 μM (P-sufficient) phosphate. Gelzan™ (0.4% w/v) was selected as gelling agent to prevent unexpected phosphate contamination from different batches of agar (Jain et al., 2009). Three days after transferring the seedlings, RH images were captured using a Nikon SMZ1500 stereomicroscope. RH length was determined by measuring at least 700 RHs located between 2 and 6 mm from the tip of the primary root in 10 individual plants for each genotype. All the measurements were repeated at least three times with representative RH images shown in the figures.

2.4 | Generation of transformants

To generate *RXR3* overexpressing lines, the *RXR3* full-length (FL) coding region was amplified from *Arabidopsis* seedling cDNA using Phusion® High-Fidelity DNA polymerase (New England Biolabs) and cloned into GATEWAY® entry vector pENTR™/SD/D-TOPO® (Invitrogen). The sequencing-confirmed vector was recombined with the pMDC32 destination vector (Curtis & Grossniklaus, 2003). For histochemical GUS analysis, a 1300-bp fragment upstream from the start codon of *RXR3* was amplified from *Arabidopsis* genomic DNA and cloned into the pBGWFS7 vector (Karimi et al., 2002). For complementation analysis of the *rxr3-1* mutant, the promoter fragment and 852-bp coding region of the *RXR3* gene was amplified and were cloned into pMU64 destination vector as described previously (Ying et al., 2022). For chromatin immunoprecipitation (ChIP) assays, the promoter fragment and FL coding region of *RSL4* were amplified from *Arabidopsis* seedling genomic DNA or cDNA and eventually recombined into the pMU64 vector, resulting in the *proRSL4::RSL4-GFP* construct. For calcium oscillation analysis, the *proUBQ10::GCAMP3* construct was transformed into individual *rxr3* mutant lines (Kwon et al., 2018).

All constructs were introduced into *Agrobacterium tumefaciens* strain GV3101 using the freeze–thaw procedure and were transformed into *Arabidopsis* by floral dipping (Zhang et al., 2006). Transformants were selected on 1/2MS agar (0.8% w/v) medium containing 25 μg ml^{-1} hygromycin (Omega Scientific).

2.5 | Western blot analysis

For detection of the green fluorescent protein (GFP) fusion protein in *RXR3* complementation plants, total protein was extracted as described previously (Ying et al., 2022). Equal amounts (30 μg) of each sample were separated by sodium dodecyl sulphate-polyacrylamide gel electrophoresis (SDS-PAGE), transferred into Immobilon-P PVDF membrane (0.45 μm; Millipore Sigma) and probed with 1/5000-diluted monoclonal mouse anti-GFP horseradish peroxidase (HRP)-conjugated antibody (Miltenyi Biotec). Chemiluminescence detection was performed with ECL™ Prime Western Blotting System (Millipore Sigma) and UVP ChemStudio imager (Analytik Jena).

2.6 | Histochemical GUS staining and GFP imaging

Histochemical GUS activity assays were performed as previously described (Jefferson et al., 1987). Briefly, seedlings were incubated in a GUS staining solution containing 100 mM sodium phosphate (pH 7.0), 1 mM ethylenediaminetetraacetic acid (EDTA), 0.05% (v/v) Triton X-100, 1 mM potassium ferricyanide/ferrocyanide and 0.5 mg ml^{-1} X-glucuronide (Goldbio) at 37°C for 1–3 h. Then, samples were then cleared in a graded series of 30%, 50%, 70% and 100% (v/v) ethanol for 30 min. Images were acquired using a Nikon SMZ1500 stereomicroscope. GFP fluorescence of the *proRXR3::RXR3-GFP* complementation plants was imaged with a Leica TCS SP8 confocal laser-scanning microscope (Ex: 488 nm; Em 507 nm).

2.7 | Measurement of RH tip $[Ca^{2+}]_{cyt}$ oscillation

To prepare *Arabidopsis* seedlings for imaging, transgenic seeds expressing the intensiometric $[Ca^{2+}]_{cyt}$ GCaMP3 reporter were directly plated on coverslips coated with a thin layer of ½MS-supplemented 0.4% Gelzan™ CM following the set-up of (Rincón-Zachary et al., 2010). After vernalization at 4°C for 2 days, Petri dishes were transferred to a growth chamber (120 μmol^{-2} s^{-1} light intensity, 22°C/20°C, 16 h light cycle and 8 h dark cycle) and were kept vertically to enable the primary root to grow down and along the surface of the gel. Growing RHs of 5-day-old seedlings were imaged with a Leica TCS SP8 confocal laser-scanning microscope (Ex: 488 nm; Em 510 nm).

For image analysis, the average fluorescence intensity was acquired by marking a rectangular region at the RH apex using the rectangular selection tool of the Leica microscope software. Fluorescence intensity values were normalized using the formula $(F - F_0)/F_0$, where F is the fluorescence intensity at any given time

point and F_0 is the lowest fluorescence intensity point for the data set (Kwon et al., 2018). $[Ca^{2+}]_{cyt}$ oscillations from the tips of at least 6 to 11 RHs from four to six seedlings of each genotype were measured.

2.8 | AtRALF1 treatment

Seedlings were germinated in a regular 1/2MS liquid medium for 5 days and then transferred to a fresh liquid medium containing 1 μM synthesized AtRALF1 peptide (49 amino acids; Pepscan). After incubating in AtRALF1-supplemented 1/2MS for 6 h, seedlings were collected for expression and fluorescence analysis. All the treatments were repeated at least two times with representative results shown in the figures.

2.9 | ChIP assay

Roots of *RSL4-GFP*-complemented seedlings, which were grown vertically on 1/2MS agar (0.8% w/v) medium for 12 days, were harvested and stored in −80°C for further steps. ChIP assays were conducted as described previously with minor modifications (Haring et al., 2007; Nelson et al., 2006; Peng et al., 2017; Saleh et al., 2008). In brief, nuclear DNA was sheared by sonication (6 s × 15 pulses, 1 min break between each pulse) and cell debris was removed by centrifugation. ChIP was performed by incubating extracted DNA with a rabbit anti-GFP polyclonal antibody (Abcam) followed by treatment with Protein A/G magnetic beads (Pierce). The beads were washed three times with high-salt wash buffer, which contained 20 mM Tris-HCl (pH 8.0), 500 mM NaCl, 0.2% (w/v) SDS, 0.5% (v/v) Triton X-100, 2 mM EDTA and the Pierce™ Protease Inhibitor mini tablet. Chromatin was eluted in buffer containing 1% (w/v) SDS and 100 mM $NaHCO_3$ and de-cross-linked at 65°C for 16 h. Cellular RNA and protein were removed by RNase (Qiagen) and proteinase-K (Applied Biosystems) treatments, respectively. Purified DNA was used as a template to determine the enrichment of target genes through PCR using primers listed in Table S2.

2.10 | CaM-binding assay

For heterologous expression of *RXR3*, its FL and N-terminal- (Δ1–22, residues 1–2, including CaM-binding domain [CaMBD]) truncated cDNA fragment was subcloned into the pMAL™-c5X vector (New England Biolabs) carrying an N-terminal maltose-binding protein (MBP) tag. For recombinant protein production, constructs were separately introduced into *Escherichia coli* (NEB Express Competent cells C2523H). Purification of RXR3 was performed using amylose resin (New England Biolabs) according to the manufacturer's instructions. Protein concentration was quantified using the Pierce™ rapid gold BCA protein assay kit (Thermo Fisher Scientific) and stored in a −80°C freezer.

CaM-binding assays were carried out according to a previous study with minor modifications (Kato et al., 2013). Briefly, recombinant MBP-$RXR3^{FL}$ or MBP-$RXR3^{\Delta 1\text{-}22}$ protein (2 μg) were incubated with 25 μl CaM-agarose (Millipore Sigma) in buffer containing 20 mM Tris (pH 7.0), 150 mM NaCl and 0.5 mM $CaCl_2$ or 2 mM EGTA for 1 h at 4°C. The supernatant was discarded by centrifugation at 1470 *g* for 2 min. After washing three times with the same buffer, bound proteins were dissociated by incubation with 2× SDS-PAGE protein sample buffer (Millipore Sigma). Samples were separated and transferred to the PVDF membrane as described above. Western blot analysis was performed using 1/5000-diluted monoclonal mouse anti-MBP-HRP antibody (Miltenyi Biotec).

2.11 | Bimolecular fluorescence complementation (BiFC) assays

BiFC analysis was performed as previously described (Kudla & Bock, 2016; Waadt et al., 2014). Briefly, *RXR3* was fused to the N-terminal EYFP in the pSITE-cEYFP or pCAMBIA1305-CFP (gift of Dr. Elison Blancaflor) vector, whereas various *Arabidopsis CaM* genes were fused to the C-terminal part of EYFP in pSITE-nEYFP. The *At3g25240/RXR1* gene was also constructed into the pSITE-cEYFP vector and used as a negative control. These different vector pairs were cotransformed into *Nicotiana benthamiana* through agroinfiltration. Forty-eight hours after infiltration, YFP or CFP fluorescence was detected using a Leica TCS SP8 confocal laser-scanning microscope (CFP, Ex: 405 nm; Em: 485 nm; YFP, Ex: 514 nm; Em: 527 nm). All the experiments were repeated at least three times with representative images shown in the figures.

2.12 | Measurement of phosphate content

Phosphate content measurement was conducted as described previously (Carter & Karl, 1982) with minor modifications. Briefly, 50 mg (fresh weight) of *Arabidopsis* tissue was ground and resuspended in 600 μl of MilliQ water. After centrifugation at 13,000 *g* for 2 min, the clarified supernatant was used to quantify phosphate content. A mixture consisting of 20 μl of supernatant, 90 μl of 1 N HCl and 90 μl of malachite green dye solution (0.042%, w/v) was incubated at room temperature for 5 min. The absorbance of the mixture at 630 nm was recorded with a spectrophotometer. The collected values were calibrated by a standard curve created with various concentrations of K_2HPO_4. All measurements were repeated at least three times with representative results shown in the figures.

2.13 | Statistical analysis

Statistical analyses and data plotting were performed with GraphPad Prism 9.0 (GraphPad Software, Inc.). Data on gene expression, RH length, shoot biomass, Pi content and amplitudes and frequencies of

$[Ca^{2+}]_{cyt}$ oscillation were analysed statistically by one-way analysis of variance with Tukey's test or Student's *t* test.

2.14 | Accession numbers

Sequence data from this article can be found in the Phytozome 12 online genomic resource (https://phytozome.jgi.doe.gov/pz/portal.html) under the following accession numbers: *AtRXR1* (*At3g25240*), *AtRabD2c* (*At4g17530*), *AtRXR3* (*At1g62420*), *Arabidopsis DUF506* gene family members (*At1g12030*, *At1g77145*, *At1g77160*, *At2g20670*, *At2g38820*, *At2g39650*, *At3g07350*, *At3g22970*, *At3g54550*, *At4g14620* and *At4g32480*), *AtCAM1* (*At5g37780*), *AtCAM2* (*At2g41110*), *AtCAM6* (*At5g21274*), AtCAM7 (*At3g43810*), AtCNGC14 (*At2g24610*), *AtRALF1* (*At1g02900*) and *AtEXPA7* (*At1g12560*).

3 | RESULTS

3.1 | Expression of *Arabidopsis DUF506* genes during P-limitation

To functionally characterize *AtDUF506* genes under P-deprivation, their expression patterns from public RNA-seq databases (i.e. GENEVESTIGATOR®) was determined. Through database searches, two additional *DUF506* genes, namely, *At2g20670* and *At3g07350*, whose expression was induced by P-limitation, were found (Table S1). Next, transcript changes of all *AtDUF506* genes in response to P-deprivation were investigated using qRT-PCR analysis (Figure 1). In addition to the two P-limitation inducible *DUF506* genes noted above, the expression of *At1g62420/RXR3* (in root) and *At4g32480* were significantly up-regulated (i.e., fold change >2) by P-limitation. Similar to *At3g25240/RXR1*, expression of *At1g62420*, *At3g07350* and *At4g32480* were induced in both shoot and root tissues, whereas *At2g20670* exhibited shoot-specific induction when exposed to P-stress. Among the *DUF506* genes, expressions of *At3g25240/RXR1*, *At1g62420* and *At3g07350* were the most P-inducible in roots (~10-fold up-regulation). Next, the tissue-specific expression pattern of *At3g07350* and *At1g62420* was analysed using promoter–GUS fusions. As shown in Figure S1, *At3g07350* expressed weakly in vascular bundles and lateral root tips under P-sufficient (control) condition. This gene was strongly induced in the entire seedling (e.g., cotyledon, primary/lateral roots and root tips) when seedlings were cultured in P-deprived liquid medium for 24 h. On the other hand, GUS activity expressed under the control of the *At1g62420* promoter was mainly observed in primary roots. Expression was strongest in vascular bundles, root tips and RHs of primary roots. In contrast, no GUS signals were detected in P-stressed shoots (Figure 2A). In P-sufficient seedlings, GUS signal

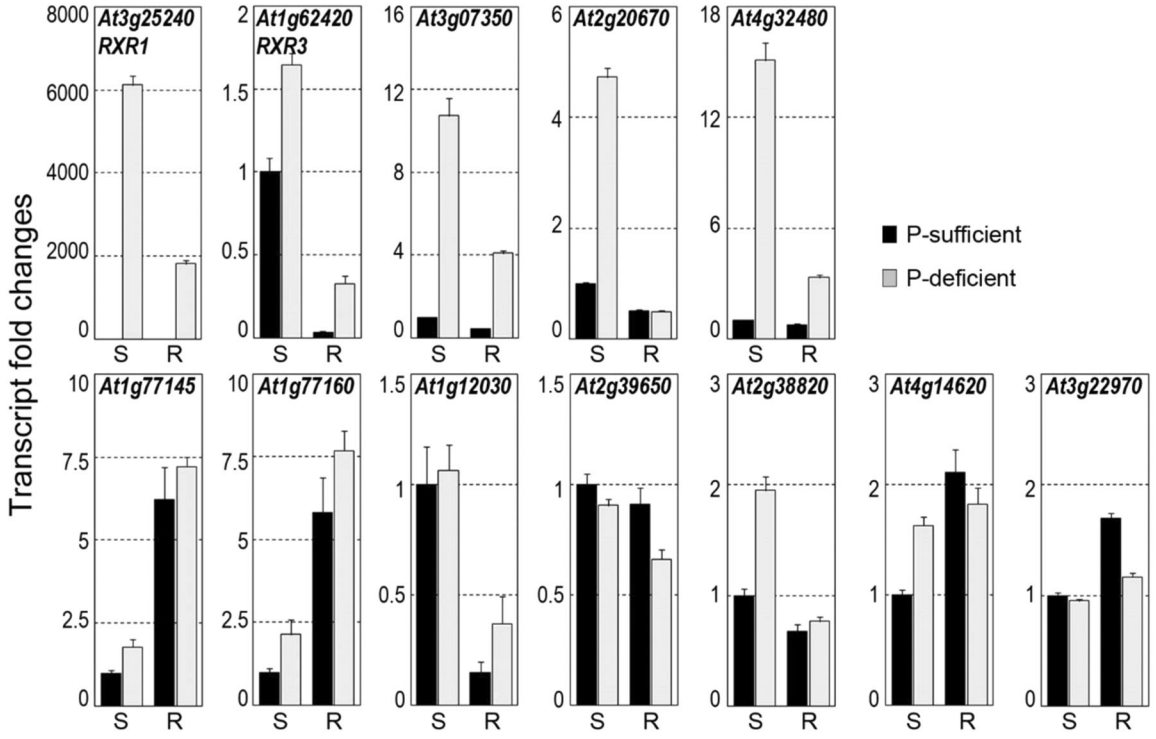

FIGURE 1 Expressions of *Arabidopsis DUF506* genes in response to P-limitation. Five-day-old WT seedlings were transferred to P-sufficient or P-deficient half-strength MS liquid medium and then the shoots and roots were harvested separately after 24 h. Expression was measured by qRT-PCR. The *At3g54550* gene was undetectable because of its silique-specific expression (Ying, 2021). The transcript level of each *DUF506* gene in shoots (P-sufficient condition) was set to 1. The *Arabidopsis GAPDH* gene was used as a reference for normalization. The data represent the mean values of three replicates ± SD. DU506, Domain of Unknown Function 506; MS, Murashige and Skoog; P, phosphorous; qRT-PCR, quantitative reverse transcription-PCR; R, root; S, shoot; WT, wild type.

was only observed in root caps. These results indicate that the levels of expression of additional *Arabidopsis DUF506* genes (i.e., *At1g62420*, *At2g20670*, *At3g07350* and *At4g32480*) respond to P-limitation and therefore their roles during P-stress warrant further investigation.

3.2 | Transcriptional characterization of P-limitation-inducible *At1g62420* gene

Because its expression is induced strongly by P-limitation in roots and it has low sequence similarity to *RXR1*, functional characterization of

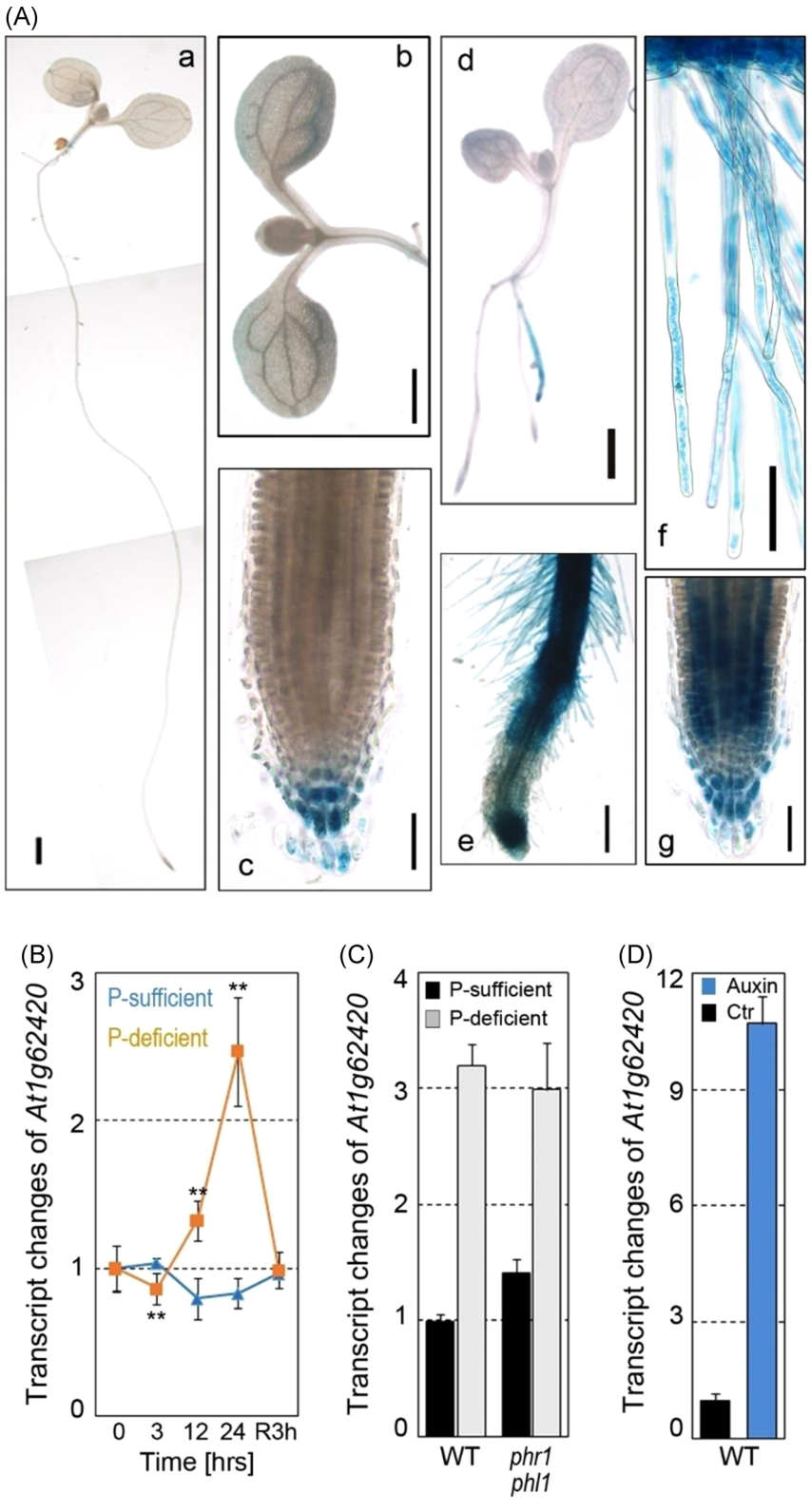

FIGURE 2 *At1g62420* responds to phosphate starvation. (A) GUS staining of the *proAt1g62420::GUS* transgenic line. Five-day-old transgenic seedlings were grown on P-sufficient (a–c) or deficient (d–g) half-strength MS solid medium for 5 days and then stained. Scale bar = 1 mm (a, b and d) or 50 µm (c, e–g). (B) Time course of *At1g62420* expression determined by qRT-PCR analysis. Five-day-old WT seedlings were transferred to fresh regular (P-sufficient) or no phosphate (P-deficient) half-strength MS liquid medium and then the samples were harvested at the indicated time points. $^{**}p < 0.01$ indicates statistical significance (P-deficient vs. P-sufficient) as determined by Student's *t* test. (C) Expression changes of *At1g62420* in roots of the *phr1 phl1* double mutant. Three-day-old seedlings were grown and treated as described in Figure 1. (D) Expression changes of *At1g62420* in wild-type roots treated with auxin (IAA). Three-day-old seedlings were transferred to P-sufficient (Control) or supplemented with 1 µM IAA in half-strength MS liquid medium. qRT-PCR analysis was performed on roots 5 days after exposure to IAA. The data represent the mean values of three replicates ± SD in panels (B–D). MS, Murashige and Skoog; P, phosphorous; qRT-PCR, quantitative reverse transcription-PCR; WT, wild type.

the *At1g62420* gene was of interest. Transcript changes of the *At1g62420* gene at various times after the onset of P-starvation were measured to determine if its response was specific to low P. Under P-sufficient conditions, the levels of *At1g62420* transcript did not change, whereas in P-stressed seedlings, *At1g62420* expression was induced after 12 h and peaked at 24 h (Figure 2B). Three hours after Pi readdition (R3h), the expression level of *At1g62420* returned to levels seen in P-sufficient conditions, indicating a direct response of *At1g62420* transcripts to plant P-status.

PHOSPHATE STARVATION RESPONSE1 (PHR1) and its homolog PHR1-LIKE (PHL1) are critical TFs in the plant P-responses (Bustos et al., 2010; Nilsson et al., 2007; Rubio et al., 2001). Because *RXR1* was transcriptionally activated by PHR1 and PHL1 (Ying et al., 2022), the regulation of *At1g62420* expression by these two TFs was studied. This was first tested by searching PHR1 binding sequences (P1BS, GNATATNC) in the *At1g62420* promoter region. No P1BS was found. Next, transcript changes of *At1g62420* in *phr1 phl1* double mutant in response to P-limitation were examined. In root tissues of *phr1 phl1* double mutant, *At1g62420* exhibited identical expression patterns as wild type (Figure 2C), indicating that its transcriptional response to P-stress was independent of PHR1 and PHL1.

During P-limitation, the concentration of endogenous auxin accumulates and redistributes in various organs. High auxin levels induce the expression of *auxin-responsive factors* (*ARFs*, e.g., *ARF5*, *7*, *8* and *19*), leading to altered root system architecture (RSA) (Bhosale et al., 2018; Mangano et al., 2017). Thus, expression changes of *At1g62420* in response to auxin treatment were investigated. Notably, three copies of the auxin-responsive element (i.e., AACGAC) were found in *At1g62420* promoter and were located in 116, 184 and 454 bp upstream of the start codon. In roots, the auxin-induced transcriptional changes of *At1g62420* (10.7 ± 0.69-fold up-regulation) were similar to those of P-stress (10.5 ± 1.38-fold up-regulation; Figures 1 and 2D). In addition, qRT-PCR indicated that transcripts of *At1g62420* were moderately reduced in *arf7 arf19* double mutant regardless of P-status (Figure S2). Collectively, results show that the transcription of *At1g62420* in roots is regulated in a manner that might be affected by but is not exclusively dependent on *ARF7/ARF19* signalling.

3.3 | *At1g62420/RXR3* represses RH growth

To elucidate the biological function of *At1g62420*, overexpression lines were generated (Figure 3A). Two independent homozygous transgenic lines (i.e., OX-5 and OX-12) exhibited significantly shorter RHs than those of wild type (e.g., P-sufficient/deficient condition, 0.189 ± 0.003/0.242 ± 0.005 mm [OX-12] vs. 0.237 ± 0.003/0.308 ± 0.004 mm [wild type]) (Figure 3C,E). Two independent T-DNA mutants (SALK_016908 and SALK_078603) were identified from ABRC (Figure 3B). qRT-PCR did not detect *At1g62420* transcript in SALK_016908 and the transcript was significantly reduced in SALK_078603 (Figure 3A). RHs of both mutants were ~40% longer than RHs of wild type under P-deficient conditions (e.g., P-sufficient/deficient condition, 0.270 ± 0.005/0.433 ± 0.007 mm [SALK_016908]; 0.299 ± 0.005/0.437 ± 0.007 mm [SALK_078603]; Figures 3C,E and S3). Because *At1g62420* mutants phenocopied the long RHs of *rxr1* (Ying et al., 2022), SALK_016908 and SALK_078603 were hereafter named *rxr3-1* and *rxr3-2*, respectively, and *At1g62420* will be referred to as *RXR3*. Additional phenotyping of the mutants under P-deficient conditions showed that *rxr3-1* had higher endogenous P-content and biomass than wild type (Figures 3I,J and S4), suggesting that RXR3 functions as an RH growth repressor that affects P-uptake and plant growth.

To ascertain that the observed RH traits were related to *RXR3* function, an endogenous promoter-driven *RXR3-GFP* construct was introduced in *rxr3-1*. GFP signal was detected in two independent complementation lines by Western blot analysis, indicating that RXR3 was correctly transcribed and translated in vivo (Figure 3G). Moreover, the RXR3-GFP was predominately detected in root epidermal cells and RH tips (Figure 3H), which points to the direct involvement of RXR3 in an RHS process. The promoter-driven *RXR3*-GFP (complemented line #1) partially rescued the long RH phenotype of *rxr3-1* (e.g., P-sufficient/deficient condition, 0.265 ± 0.004/0.362 ± 0.007 mm [complemented line #1] vs. 0.233 ± 0.004/0.327 ± 0.006 mm [wild type]; Figures 3D,F and S3).

Because loss-of-function *RXR1* and *RXR3* led to longer RHs, *rxr1 rxr3-1* double mutants were generated to determine if they genetically interact during RH development (Figure 4). Under P-sufficient condition, RHs of *rxr1 rxr3-1*double mutant (0.360 ± 0.005 mm) was comparable to *rxr1* (0.366 ± 0.006 mm), but significantly longer than *rxr3-1* (0.309 ± 0.005 mm) and wild type (0.256 ± 0.004 mm). Under P-deficient conditions, the double mutant (0.456 ± 0.007 mm) exhibited significantly longer RHs ($p < 0.01$) than either one of the single mutants, suggesting an additive function (*rxr1*, 0.421 ± 0.007 mm; *rxr3-1*, 0.430 ± 0.006 mm). Taken together, the double mutant studies indicate that RXR3 inhibits RH growth through a pathway that is independent of RXR1.

3.4 | RXR3 is directly regulated by RSL4

RSL4 is a critical TF that specifies RH initiation and elongation by modulating the expression of several RH-related genes (Yi et al., 2010). Therefore, it was hypothesized that *RXR3* expression could be regulated by RSL4. RSL4 binds to RHEs in the promoter regions of RH-expressed genes (Hwang et al., 2017). Four RHEs were identified in the *RXR3* promoter region (Figure 5A) and the P-limitation-inducible expression of *RXR3* was not observed in *rsl4* (Figure 5B). These findings suggest that RSL4 might directly bind to RHEs of *RXR3* to regulate its expression. In doing so, RSL4 and RXR3 could synergistically control RH growth under P-limitation. To test the hypothesis that RSL4 binds to RHEs in *RXR3* promoter, *RSL4* expression was examined in response to P-limitation or auxin. As shown in Figure S5, *RSL4* transcripts in roots were induced (~2-fold) by both treatments. Next, an endogenous promoter-driven *RSL4-GFP*

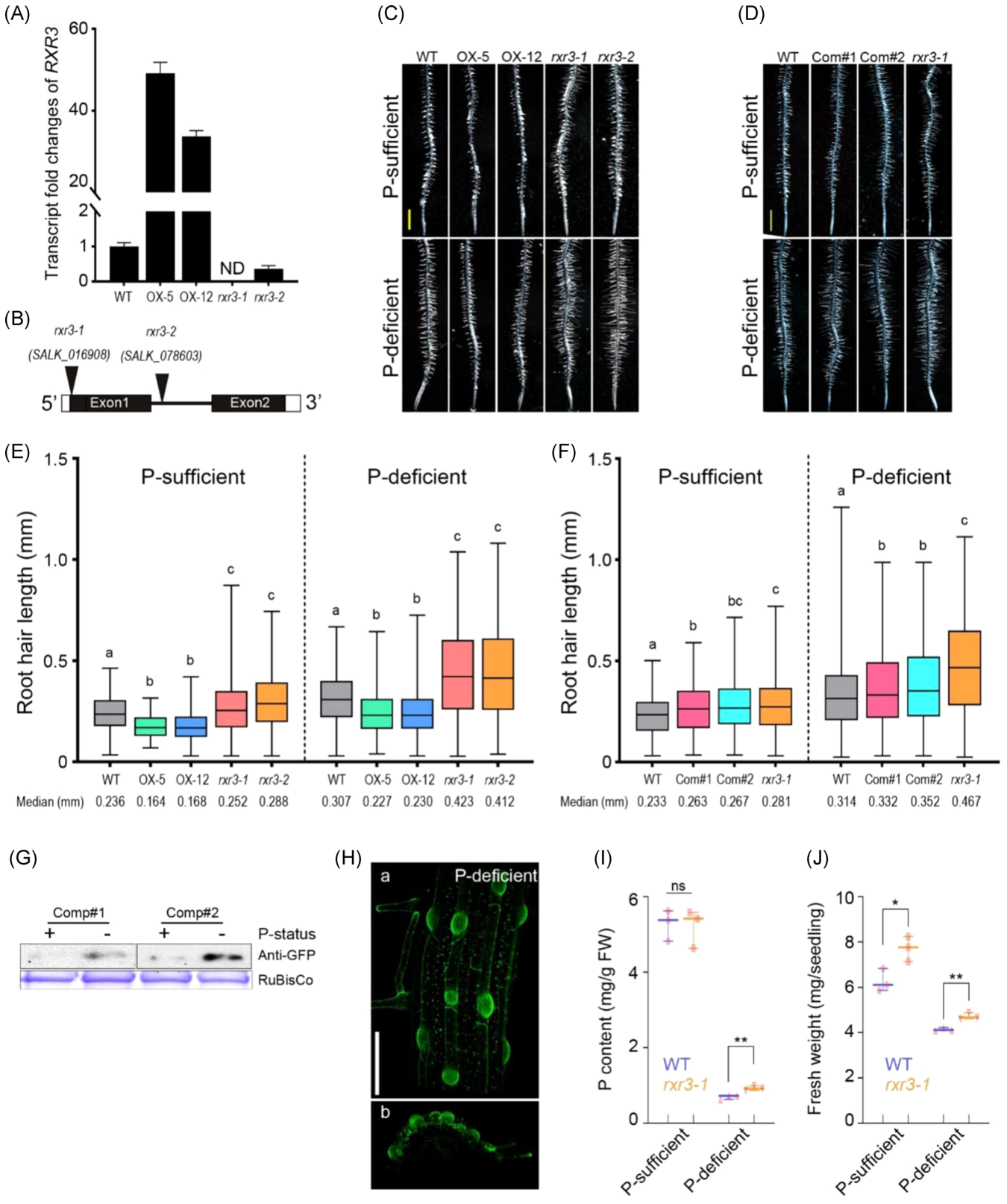

FIGURE 3 (See caption on next page)

was expressed in *rsl4*. The RH phenotype of the complemented *rsl4* mutant was similar to the one of wild type, indicating that the RSL4-GFP fusion protein rescued the *loss-of-function* RH phenotype of *rsl4* (Figure S6). ChIP analysis was then conducted to determine whether RSL4 binds to the RHEs in *RXR3* promoter. *EXPANSIN A7* (*EXPA7*) is a well-known RSL4-regulated gene (Yi et al., 2010); therefore, it was used as a positive control in the ChIP assays (Figure S7). As shown in Figure 5C, RSL4 interacted with probes 2 and 3, which contained

RHE motifs of *RXR3* (Figure 5A). No interaction was observed between RSL4 and probe 1, which did not have *RXR3* RHEs. These results suggest that RSL4 directly binds to RHEs within the *RXR3* promoter.

Recently, Zhu et al. (2020) proposed that the peptide RALF1 and the leucine-rich receptor-like kinase, FERONIA (FER), play central roles in RH growth. One mechanism by which RALF1 governs FER-mediated RH growth is through translational regulation of RSL4 by FER-phosphorylated eIF4E1. Although *RALF1* was insensitive to P-limitation (Table S1), it was hypothesized that RALF1 treatment might simulate P-starvation to activate RSL4, and consequently lead to *RXR3* transcript accumulation. To test this hypothesis, 5-day-old *RXR3* promoter-GUS or *rxr3-1* complemented seedlings were incubated with 1/2MS liquid medium supplemented with 1 μM

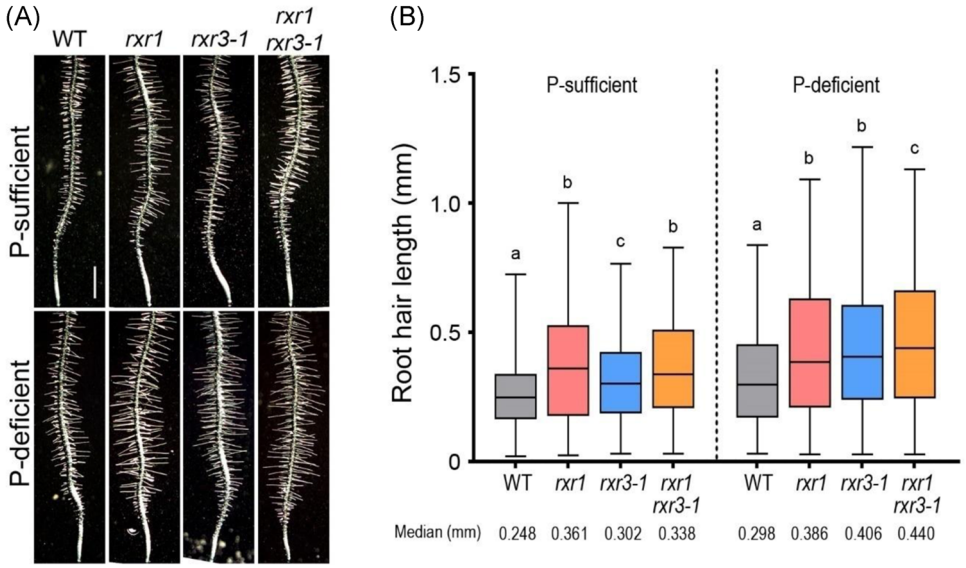

FIGURE 4 Root hair phenotype of *rxr1* and *rxr3-1* single mutants, and *rxr1 rxr3* double mutant. (A) Representative root hair images of 5-day-old seedlings. Scale bar = 1 mm. (B) Box plots of root hair lengths in WT, *rxr1* and *rxr3-1* single mutants and *rxr1 rxr3* double mutant, under P-sufficient or P-deficient condition. Box limits indicate 25th and 75th percentiles, horizontal line is the median and whiskers display the minimum and maximum values. Between 906 and 1037 root hairs from 10 seedlings were measured for each genotype and numbers at the bottom indicate median values (in mm) for each genotype. Statistical significance of differences was tested by one-way ANOVA analysis ($p < 0.001$) and is indicated by lower case letters. ANOVA, analysis of variance; P, phosphorous; WT, wild type.

FIGURE 3 *RXR3* represses *Arabidopsis* root hair elongation. (A) qRT-PCR analysis of *RXR3* transcript level in *RXR3* overexpressers or *rxr3* mutants, under P-sufficient condition.ND, not detectable. (B) Schematic diagram of two T-DNA insertion mutants used in the study. Exons, black boxes; UTRs, white boxes; intron, black line. (C and D) Representative images showing the effect of *RXR3* on root hair elongation. Three-day-old seedlings were transferred to P-sufficient or P-deficient half-strength MS solid medium and then grown vertically for 2 days. While the *loss-of-function* mutants (*rxr3-1* and *rxr3-2*) grow longer root hairs, constitutive overexpression of *RXR3* (*proCaMV35S::RXR3*, OX-5 and 12) represses root hair growth (c). Root hair growth is restored to wild-type levels in *rxr3-1* mutants complemented with *RXR3* (*proRXR3::RXR3-GFP*, Com#1 and #2; d). Scale bar = 1 mm. (E and F) Box plots of root hair lengths in WT, *RXR3* overexpressers, *rxr3* mutants and complemented lines, under P-sufficient or P-deficient condition. Box limits indicate 25th and 75th percentiles, horizontal line is the median and whiskers display the minimum and maximum values. Between 885 and 1026 root hairs from 10 seedlings were measured for each genotype and numbers at the bottom indicate median values (in mm) for each genotype. Statistical significance of differences was tested by one-way ANOVA Tukey's analysis ($p < 0.001$). Means with different letters indicated statistical significance. (G) Immunoblot analysis of RXR3-GFP fusion protein in complementation lines (#1 and #2) under different P-conditions. Coomassie blue-stained RuBisCO protein is shown as a loading control. (H) Initiating root hairs (a) and root epidermal (b, transverse view) showing the localization of RXR3-GFP fusion protein in *Arabidopsis* complemented line (Comp#1) under P-stress. Scale bar = 100 μm. (I and J) Box plots of shoot phosphate content (I) or fresh biomass (J) of 10-day-old wild type (blue) and *rxr3-1* mutant (orange) seedlings grown on P-sufficient or P-deficient half-strength MS solid medium ($n = 3$). Horizontal line is the median and whiskers that display the minimum and maximum values. (I and J) $^{**}p < 0.01$ or $^{*}p < 0.05$ indicates statistical significance as determined by Student's *t* test. ANOVA, analysis of variance; GFP, green fluorescent protein; MS, Murashige and Skoog; ND, not determined; ns, no significance; P, phosphorous; qRT-PCR, quantitative reverse transcription-PCR; Rubisco, ribulose 1,5-bisphosphate carboxylase/oxygenase; UTR, untranslated region; WT, wild type.

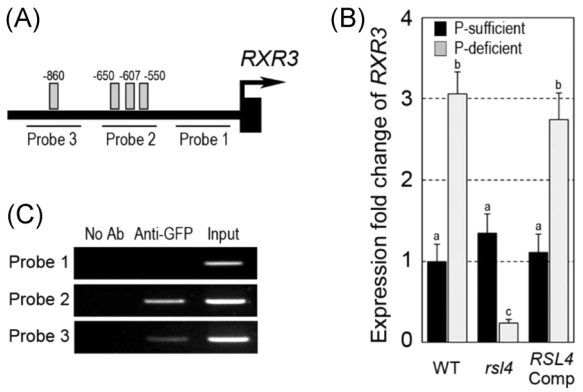

FIGURE 5 RSL4 binds to the *RXR3* promoter. (A) Schematic diagram of the *RXR3* promoter region showing the relative positions of RHEs. The RHEs ($TN_6CA[CT]G[TA]$) are marked by grey rectangles, and relative positions and sizes of the different PCR-amplified fragments are indicated by black lines under the RHE(s). (B) qRT-PCR analysis of *RXR3* expression in *rsl4* mutants and complementation lines. Three-day-old *Arabidopsis* seedlings were transferred to fresh P-sufficient or deficient half-strength MS liquid medium. qRT-PCR assays were done on roots after 24 h. The data represent the mean values of three replicates ± SD. Statistical significance of differences was tested by one-way ANOVA analysis ($p < 0.01$) and is indicated by lower case letters. (C) ChIP analysis to detect the association between RSL4 and the RHEs within the *RXR3* promoter in the RSL4-GFP transgenic line. The ChIP signals with (anti-GFP) and without (No Ab) addition of anti-GFP are indicated. Ab, antibodies; ANOVA, analysis of variance; ChIP, chromatin immunoprecipitation; GFP, green fluorescent protein; qRT-PCR, quantitative reverse transcription-PCR; RHE, root hair element.

RALF1 for 6 h. As shown in Figure 6A,B, *RXR3* exhibited the same expression pattern in the root epidermis in response to RALF1 as that of P-stress (Figure 3H). Furthermore, *RXR3* transcript in wild type and RSL4 complemented line was induced by RALF1 treatment, but not in *rsl4* mutants (Figure 6C). These results support the hypothesis that *RXR3* expression is transcriptionally regulated by RSL4 through pathways that intersect with RALF1.

3.5 | RXR3 interacts with CaMs

In contrast to RXR1 (Ying et al., 2022), RXR3 has an N-terminal CaMBD between amino acids 11 and 22 (motif 1–12, [FILVW] xxxxxxxxxx[FILVW]), in addition to the DUF506 domains that define the protein family. This observation led to the hypothesis that RXR3 might interact with CaMs. This was tested by heterogeneously expressing and purifying MBP-tagged recombinant RXR3 protein ($MBP\text{-}RXR3^{FL}$), and N-terminally truncated mutant ($MBP\text{-}RXR3^{\Delta1-22}$, lack of CaMBD; Figures 7A and S8). These recombinant proteins were separately incubated with CaM-agarose in the presence or absence of Ca^{2+}. The bound protein was dissociated, subjected to SDS-PAGE and detected by immunoblotting with antibodies against the MBP tag. As shown in Figure 7B, $RXR3^{FL}$ bound to CaM-agarose in the presence of Ca^{2+}, but not in the presence of Ca^{2+} chelator, EGTA. By contrast, $RXR3^{\Delta1-22}$ did not bind to CaM-agarose, in the presence of Ca^{2+}. These results indicate that the N-terminal CaMBD of RXR3 is required and sufficient for binding to the Ca^{2+}–CaM complex.

To validate the interaction between RXR3 and CaMs in vivo, BiFC assays were conducted. In *Arabidopsis*, there are four isoforms of CaM (e.g., CaM1/4, CaM2/3/5, CaM6 and CaM7) that derive from seven CaM encoding genes (Bender & Snedden, 2013; Zielinski, 1998). Four of the seven *CaM* genes (i.e., *CaM1*, *CaM2*, *CaM6* and *CaM7*) were selected for the BiFC assays with RXR3. Strong cytosolic yellow fluorescence was observed in RXR3-CaM1, RXR3-CaM2, RXR3-CaM6 and RXR3-CaM7 pairs, but not the RXR1-CaM7 (negative control) pair (Figures 7C and S9). Overall, in vitro binding and in vivo BiFC assays demonstrate that RXR3 physically interacts with Ca^{2+}–CaMs.

3.6 | RXR3 influences RH tip $[Ca^{2+}]_{cyt}$ oscillation

CaMs function as versatile Ca^{2+}-binding proteins that regulate the activity of numerous effectors (e.g., CNGCs) in Ca^{2+} signalling. Multiple CNGCs (e.g., CNGC6/9/14) generate and maintain RH tip-focused $[Ca^{2+}]_{cyt}$ oscillations (Brost et al., 2019). It was reported that CaM7 associates with CNGC14 to regulate RH polar growth presumably by controlling Ca^{2+} influx (Zeb et al., 2020). Therefore, we hypothesized that the interaction of RXR3 and CaM7 could inhibit or disrupt the CaM7–CNGC14 association. If so, RXR3 exerts its inhibitory function by regulating the affinity of CaM7 to CNGC14. When RXR3-CFP was coexpressed with CaM7-nEYFP and CNGC14-cEYFP in tobacco, yellow fluorescence was not affected (Figure 8A,B). RXR3 not only colocalized with the CNCG14–CaM7 complex in the cytosol but also was found in the nucleus (arrow, Figure 8B). These results indicate that RXR3 did not interfere with the interaction between CaM7 and CNGC14, and might conduct other functions in the nucleus. Furthermore, the GCaMP3 construct was expressed in wild type, *rxr3-1* and *rxr3-2* to determine whether RXR3 influences RH apical $[Ca^{2+}]_{cyt}$ oscillations (Figures 8C–E, S10 and S11 and Supporting Information Video S1). Both *rxr3* mutants (*rxr3-1*, 0.0517 ± 0.0027 Hz; *rxr3-2*, 0.0542 ± 0.0020 Hz) exhibited ~20% higher frequencies of $[Ca^{2+}]_{cyt}$ oscillation than wild type (0.0399 ± 0.0009 Hz). Moreover, the amplitude of $[Ca^{2+}]_{cyt}$ oscillation was dampened (~40%) in *rxr3-1*. These results suggest that RXR3 represses RH growth possibly by regulating $[Ca^{2+}]_{cyt}$ oscillations. However, it cannot be ruled out that the observed disruptions in $[Ca^{2+}]_{cyt}$ oscillations in *rxr3* are secondary effects caused by altered RH growth.

Overexpression of *CaM7* represses RH growth by inhibiting CNGC14 activity (Zeb et al., 2020), which phenocopies *RXR3* overexpressers. This led to the hypothesis that *cam7* mutant might also phenocopy the long RHs of *rxr3*. Similar to *rxr3*, RHs of *cam7* were longer than those of wild type (Figure S12). Additionally, to investigate whether RXR3 and CaM7 function in a similar pathway,

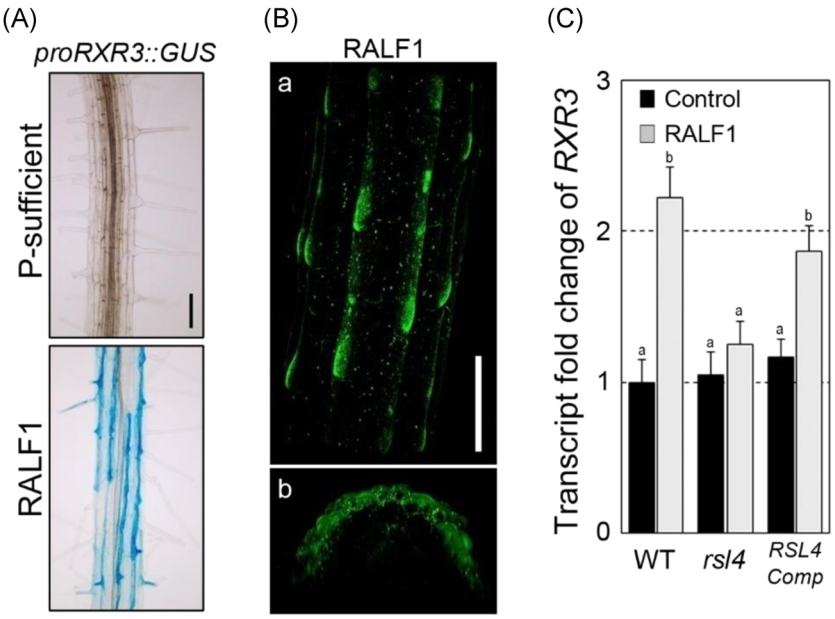

FIGURE 6 RSL4 is required for *RXR3* expression. Five-day-old seedlings were transferred to control (P sufficient), or supplemented with 1 μM RALF1 half-strength MS liquid medium. After incubation for 6 h, root tissues were harvested for analysis. (A) GUS staining of *proRXR3::GUS* roots after RALF1 treatment. Scale bar = 100 μm. (B) Initiating root hairs (a) and root epidermal (b, transverse view) localization of RXR3-GFP fusion protein in *Arabidopsis* complemented line (Comp #1) after RALF1 treatment. Scale bar = 100 μm. (C) qRT-PCR analysis of *RXR3* expression in *rsl4* mutants and its complementation line, after RALF1 treatment. The data represent the mean values of three replicates ± SD. Statistical significance of differences was tested by one-way ANOVA analysis ($p < 0.01$) and is indicated by lower case letters. ANOVA, analysis of variance; MS, Murashige and Skoog; P, phosphorous.

$RXR3^{FL}$ was overexpressed in *cam7*. $RXR3^{FL}$ Overexpression did not reverse the long RH phenotype of *cam7* (Figure S12). Based on these results, CaM7 might function upstream of RXR3 to affect RH growth and apical $[Ca^{2+}]_{cyt}$ oscillation.

4 | DISCUSSION

Many proteins with domains of unknown function (DUF) were identified and annotated, but remain to be functionally characterized (Ying, 2021). Recently, we demonstrated that *Arabidopsis* P-limitation-inducible DUF506 protein, *AT3G25240/RXR1*, negatively regulates RH growth by interacting with the small GTPase RabD2c (Ying et al., 2022). Here, we report four additional P-limitation-inducible *DUF506* genes in *Arabidopsis* and show that one of these DUF506-containing proteins, RXR3, is another repressor of RH elongation growth.

Because their expression is strongly induced by low P, we investigated two *AtDUF506* genes in more depth. *At3g07350*, which is the segmental duplication of *RXR1* (Ying, 2021), is an uncharacterized and putative RH specific gene with two RHE in its promoter region (Won et al., 2009). Here, GUS staining revealed that under P-stress, *At3g07350* expression is highly induced in roots, most notably in root tips and RHs (Figure S1). Moreover, the expression analysis revealed that *At3g07350* in throot was induced by auxin (~3-fold upregulation; Figure S13), suggesting that it is involved in auxin-dependent regulatory pathways. Collectively, the data indicate that *At3g07350* functions through an auxin-mediated P-signalling pathway, independent of *RXR1*.

To unravel the biological function of *RXR3* gene, we performed genetic, biochemical and cytological experiments (Figures 2–8). Because the *RXR3* expression pattern based on GUS and qRT-PCR analysis mirrored the one of *RXR1*, we hypothesized that RXR3 might also function as a redundant RH growth repressor. Consistent with this hypothesis was the finding that overexpression of *RXR3* reduced RH lengths, whereas *loss-of-function* mutants exhibited longer RHs than wild type (Figure 3). The shorter and longer RHs of *RXR3* overexpressors and *rxr3*, respectively, are reminiscent of how RXR1 affects RH growth. Although RXR1 and RXR3 have similar repressor functions on RH growth, the results of this study revealed that the mechanism by which RXR3 influences RH development is distinct from that of RXR1. For instance, *RXR1* responds to P-stress by a >1000-fold upregulation of its expression through PHR1/PHL1-dependent and auxin-independent pathways (Ying et al., 2022). By contrast, *RXR3* influenced RH growth through PHR1/PHL1-independent pathways and was induced by auxin (Figure 2). Furthermore, under P-deficient conditions, the *rxr1 rxr3-1* double mutant exhibited longer RHs than both single mutants (Figure 4). Taken together, the data indicate functional and regulatory divergence of RXR1 and RXR3.

RSL4 expression is up-regulated by P-limitation and its overexpression promotes RH growth (Figure S5) (Bhosale et al., 2018; Datta et al., 2015; Yi et al., 2010). Here, we demonstrate that RSL4

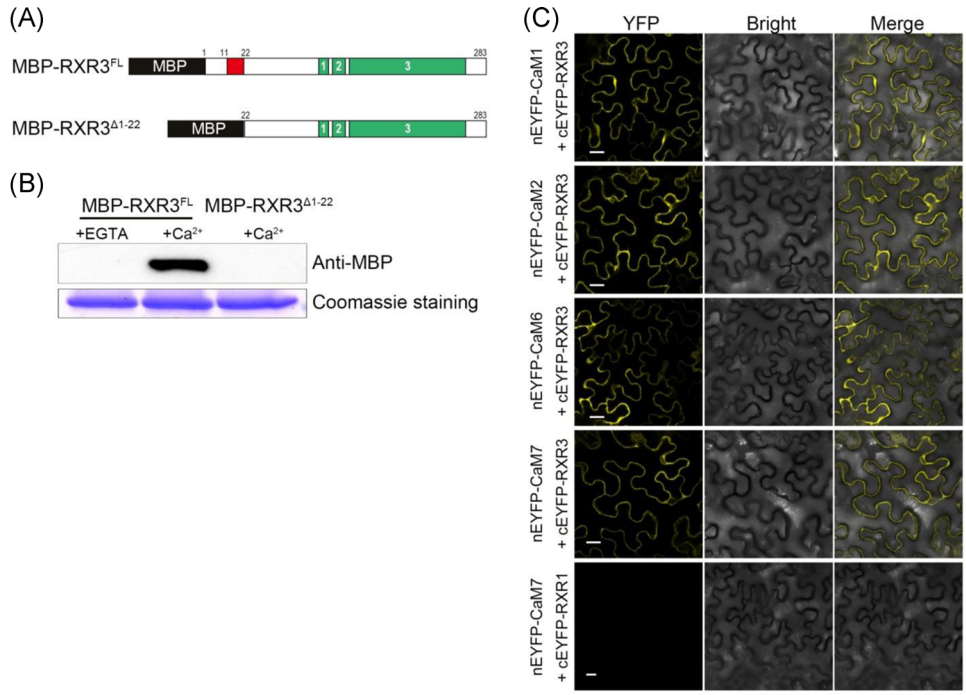

FIGURE 7 RXR3 interacts with calmodulins (CaMs). (A) Diagram of full-length (FL) RXR3 protein tagged with maltose-binding protein (MBP, black boxes) and its truncated mutant (Δ1–22), which lacks the CaM-binding domain (CaMBD, red box). Green boxes indicate the three conserved motifs present in the plant DUF506 family (Ying et al., 2022). (B) Immunoblot analysis of recombinant MBP-RXR3^{FL} and MBP-RXR3$^{\Delta1-22}$ protein binding with CaM-agarose in the presence or absence of Ca^{2+}. Recombinant protein (2 μg each) was incubated with CaM-agarose in the presence of 0.5 mM Ca^{2+} or 2 mM EGTA. Proteins bound to the CaM-agarose were separated by SDS-PAGE gel and detected by immunoblotting with anti-MBP tag antibody. Coomassie blue-stained recombinant protein (10% input) is shown as the loading control. (C) BiFC analysis to detect the interaction between RXR3 and CaMs in *Nicotiana benthamiana*. FL *RXR3* or *RXR1* (as negative control) and various *CaM* genes were cloned into pSITE-cEYFP or pSITE-nEYFP vectors. Constructs were cotransformed into *N. benthamiana* leaves via syringe infiltration. All the measurements were repeated at least three times with representative results shown. Scale bar = 20 μm. BiFC, bimolecular fluorescence complementation; $[Ca^{2+}]_{cyt}$, cytosolic Ca^{2+}; CFP, cyan fluorescent protein; DUF506, Domain of Unknown Function 506; SDS-PAGE, sodium dodecyl sulphate–polyacrylamide gel electrophoresis; YFP, yellow fluorescence protein.

binds to RHE motifs in the *RXR3* promoter, which results in the accumulation of *RXR3* transcript (Figure 5). Zhu et al. (2020) propose an autocrine signalling pathway, which includes RALF1-FER-RSL4, to synergistically regulate RH size. We found that RALF1 activates RSL4, indicating that the accumulation of *RXR3* transcript is directed by RSL4 TF (Figure 6). Given that auxin induces *RXR3* expression (Figures 2D and S2), we conclude that RXR3 participates in auxin-dependent and RSL4-mediated signalling pathways, to manage P-limitation-induced RH elongation (Figure 9).

Ca^{2+} is a second messenger that transduces signals by associating with various Ca^{2+} binding proteins (e.g., CaM and CDPK). Ca^{2+} binds to EF-hand motifs of Ca^{2+} binding proteins to modulate many biological processes in plants (Hepler, 2005; Himschoot et al., 2015; Thor, 2019; Yuan et al., 2017). Accumulating evidence suggests that tip-focused oscillations of intracellular Ca^{2+} concentration ($[Ca^{2+}]_{cyt}$) are critical for sustained RH growth (Bibikova et al., 1997; W. Feng et al., 2018; Konrad et al., 2011; Monshausen et al., 2008). CNGC14 was reported to stabilize the integrity of growing RHs, support cell expansion and interact with CaM7 to inhibit RH tip growth (Brost et al., 2019; Zeb et al., 2020; Zhang et al., 2017). CaMBDs were identified in most *Arabidopsis* DUF506 members (S. Ying, 2021). Protein microarray analysis demonstrated that DUF506 protein At1g77145 binds to several CaM or CML proteins (Popescu et al., 2007). Here, BiFC and CaM-binding assays revealed that RXR3 is also a CaM-interacting DUF506 protein (Figure 7). Overexpression of *RXR3*$^{\Delta1-22}$ (CaMBD-truncated mutant) in *rxr3-2* did not restore its long RH phenotype (Figure S14), indicating that the CaMBD is critical for inhibiting RH growth. Moreover, the association between CaM7 and CNGC14 was not noticeably affected by RXR3 (Figure 8A,B). The long RH phenotype of *cam7* was not reversed by constitutively overexpressing the *RXR3* gene (Figure S12), demonstrating that *CaM7* is required for the inhibitory role of *RXR3* on RH growth. It is notable that the transcript and protein level of RXR3 were significantly induced by P-stress (Figures 2 and 3G). Thus, whether the P-limitation-induced accumulation of RXR3 protein affects the CaM–CNGC14 interaction requires further investigation.

In addition to CNGC14, other CNGCs are important regulators of RH or pollen tube tip growth (Brost et al., 2019; Chang et al., 2007; Gao et al., 2016; Pan et al., 2019; Tan et al., 2020; Tunc-Ozdemir et al., 2013; Zhang et al., 2017). Some CNGCs spontaneously form heteromeric complexes, such as CNGC9/14 and CNGC2/4, to conduct their regulatory roles (Brost et al.,

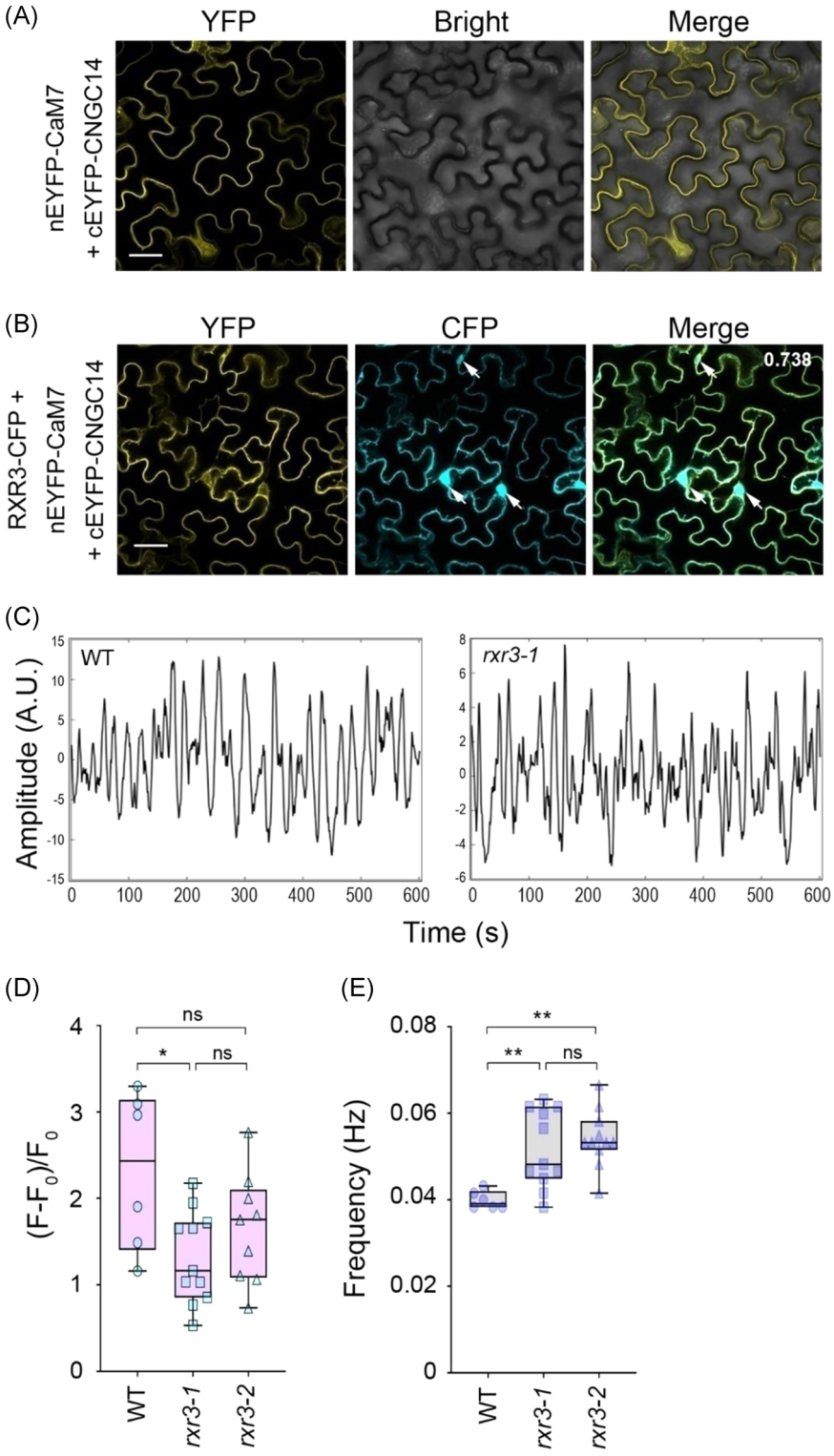

FIGURE 8 RXR3 affects root hair apical $[Ca^{2+}]_{cyt}$ oscillation. (A) BiFC analysis reveals an interaction between CNGC14 and CaM7 in *Nicotiana benthamiana*. (B) BiFC analysis shows that interaction between CNGC14 and CaM7 is independent of RXR3. Arrow, nucleus. Scale bar = 20 µm (A and B). Number in the top right corner of (B) indicates Pearson's coefficient that is calculated by ImageJ/JACoP Plug-in. (C) Representative normalized root hair $[Ca^{2+}]$ oscillograms of wild type (WT) and *rxr3-1* mutant. The data were processed by baseline simulation analysis. (D and E) Box plot of $[Ca^{2+}]_{cyt}$ oscillation amplitudes (D) or frequencies (E) in root hairs of *rxr3* mutants and WT over 600 s. Box limits indicate 25th and 75th percentiles, horizontal line is the median and whiskers display the minimum and maximum values. Each semitransparent dot represents individual measurements from 6 to 11 root hairs per group from 4 to 6 plants. $^{**}p < 0.01$ and $^{*}p < 0.05$ indicates statistical significance as determined by one-way ANOVA analysis. ANOVA, analysis of variance; BiFC, bimolecular fluorescence complementation; $[Ca^{2+}]_{cyt}$, cytosolic Ca^{2+}; CaM, calmodulin; CFP, cyan fluorescent protein; ns, no significance; YFP, yellow fluorescence protein.

2019; Chin et al., 2013; Yu et al., 2019). In contrast to CaM7-arrested CNGC14, the activity of CNGCs is positively regulated by CaM binding (e.g., CaM1 to CNGC12) (Dietrich et al., 2020; Jarratt-Barnham et al., 2021). Such studies shed light on the diverse regulatory mechanisms of CNGC. From the current work and previous reports, at least two of DUF506 proteins (i.e., At1g77145 and RXR3) interact with CaMs. Future studies will investigate how these interactions affect CNGC activity or intrinsic Ca^{2+} dynamics.

To assess the influence of *RXR3* on RH tip-focused Ca^{2+} dynamics, the GCaMP3 construct was introduced into two individual *rxr3* mutant lines, and the $[Ca^{2+}]_{cyt}$ oscillations in RH apex were recorded (Figures 8C–E, S10 and S11 and Supporting Information Video S1). The altered Ca^{2+} oscillations in tips of

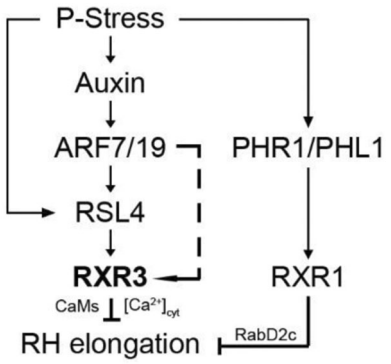

FIGURE 9 Proposed working model illustrating the different pathways by which RXR1 and RXR3 repress root hair elongation. Under P-stress, *RXR3* is transcriptionally activated by auxin through RSL4 TF, whereas *RXR1* participates in the PHR1/PHL1-dependent pathway. RXR1 interacts with RabD2c GTPase to inhibit RH elongation (Ying et al., 2022). In contrast, RXR3 binds to Ca^{2+}-activated CaMs to regulate tip-focused $[Ca^{2+}]_{cyt}$ oscillations and eventually RH growth. Blunt end, negative action; arrow, positive action; solid line, experimentally supported; broken line, hypothetical. $[Ca^{2+}]_{cyt}$, cytosolic Ca^{2+}; CaM, calmodulin; RH, root hairs; TF, transcription factor.

growing RHs of *rxr3* mutant, such as dampened amplitude and elevated frequency, indicated that RXR3 disturbed RH tip-focused $[Ca^{2+}]_{cyt}$ gradients. The RH phenotype and tip-focused Ca^{2+} oscillations of *rxr3* mutants are opposite to those of the *eru* mutant. The *ERU* gene encodes an RH-specific plasma membrane-localized receptor-like kinase and is regulated by ARF7 and ARF19 (Schoenaers et al., 2018). A recent study reveals that ERU regulates RH growth through RH tip $[Ca^{2+}]_{cyt}$ oscillations (Kwon et al., 2018). Our current findings support the notion that RXR3 negatively regulates RH growth, albeit the mechanisms affecting RH tip Ca^{2+} oscillations are still unclear. Note that GCaMP3 is a nonratiometric Ca^{2+}sensor and is therefore less suitable to derive relative differences (e.g., amplitude) in [Ca2+]cyt. Alternative ratiometric Ca^{2+} biosensors, such as the Yellow Cameleon (YC) 3.6, could present a more accurate picture of the differences between Ca^{2+} oscillations in RH tips of wild type and *rxr3*. It is also notable that the frequency of $[Ca^{2+}]_{cyt}$ oscillation in RH tips of *rxr1* is higher than the one of wild type (Ying et al., 2022). Therefore, the possibility that RabD2c and RXR3 interact cannot be excluded, because of the omnipresence of the conserved domain 3 in the DUF506 family. On the other hand, our results substantiate previous findings that elements outside the conserved domain of DUF506 proteins are essential for their regulatory functions (Ying et al., 2022).

In summary, this study supports a model in which RXR3 has inhibitory functions that are essential for the maintenance of P-limitation-induced RH growth (Figure 9). It remains to be determined whether and/or how RXR3 connects with the other tip growth-focused CNGCs. Taken together with previous studies, our data suggest that RXR1 and RXR3 function as novel components of the P-limitation-inducible RH growth regulatory network.

ACKNOWLEDGEMENTS

We thank Dr. Elison Blancaflor for providing plasmids, *rsl4* mutant seeds, advice in operating microscopes, Ca^{2+} imaging and critical comments on the manuscript. We also thank Fuqi Liao for the measurement of RH length and calcium oscillation, Sylvia Warner for technical assistance and Dr. Marcus Griffiths (Donald Danforth Plant Science Center) for comments. The work was funded by the Noble Research Institute LLC.

CONFLICTS OF INTEREST

The authors declare no conflicts of interest.

DATA AVAILABILITY STATEMENT

All relevant data can be found within the manuscript and its Supporting Information Materials.

REFERENCE

Abarca, A., Franck, C.M. & Zipfel, C. (2021) Family-wide evaluation of RAPID ALKALINIZATION FACTOR peptides. *Plant Physiology*, 187, 996–1010. Available from: https://doi.org/10.1093/plphys/kiab308

Bates, T.R. & Lynch, J.P. (2001) Root hairs confer a competitive advantage under low phosphorus availability. *Plant and Soil*, 236(2), 243–250. Available from: https://doi.org/10.1023/A:1012791706800

Bender, K.W. & Snedden, W.A. (2013) Calmodulin-related proteins step out from the shadow of their namesake. *Plant Physiology*, 163(2), 486–495. Available from: https://doi.org/10.1104/pp.113.221069

Bhosale, R., Giri, J., Pandey, B.K., Giehl, R., Hartmann, A., Traini, R. et al. (2018) A mechanistic framework for auxin dependent *Arabidopsis* root hair elongation to low external phosphate. *Nature Communications*, 9(1), 1409. Available from: https://doi.org/10.1038/s41467-018-03851-3

Bibikova, T.N., Zhigilei, A. & Gilroy, S. (1997) Root hair growth in *Arabidopsis thaliana* is directed by calcium and an endogenous polarity. *Planta*, 203(4), 495–505. Available from: https://doi.org/10.1007/s004250050219

Brost, C., Studtrucker, T., Reimann, R., Denninger, P., Czekalla, J., Krebs, M. et al. (2019) Multiple cyclic nucleotide-gated channels coordinate calcium oscillations and polar growth of root hairs. *The Plant Journal*, 99(5), 910–923. Available from: https://doi.org/10.1111/tpj.14371

Brown, L.K., George, T.S., Dupuy, L.X. & White, P.J. (2013) A conceptual model of root hair ideotypes for future agricultural environments: what combination of traits should be targeted to cope with limited P availability? *Annals of Botany*, 112(2), 317–330. Available from: https://doi.org/10.1093/aob/mcs231

Bucher, M. (2007) Functional biology of plant phosphate uptake at root and mycorrhiza interfaces. *New Phytologist*, 173(1), 11–26. Available from: https://doi.org/10.1111/j.1469-8137.2006.01935.x

Bustos, R., Castrillo, G., Linhares, F., Puga, M.I., Rubio, V., Pérez-Pérez, J. et al. (2010) A central regulatory system largely controls transcriptional activation and repression responses to phosphate starvation in *Arabidopsis*. *PLoS Genetics*, 6(9), e1001102. Available from: https://doi.org/10.1371/journal.pgen.1001102

Carter, S.G. & Karl, D.W. (1982) Inorganic phosphate assay with malachite green: an improvement and evaluation. *Journal of Biochemical and Biophysical Methods*, 7(1), 7–13. Available from: https://doi.org/10.1016/0165-022X(82)90031-8

Chang, F., Yan, A., Zhao, L.-N., Wu, W.-H. & Yang, Z. (2007) A putative calcium-permeable cyclic nucleotide-gated channel, CNGC18, regulates polarized pollen tube growth. *Journal of Integrative Plant Biology*, 49(8), 1261–1270. Available from: https://doi.org/10.1111/j.1672-9072.2007.00524.x

Chin, K., DeFalco, T.A., Moeder, W. & Yoshioka, K. (2013) The Arabidopsis cyclic nucleotide-gated ion channels AtCNGC2 and AtCNGC4 work in the same signaling pathway to regulate pathogen defense and floral transition. *Plant Physiology*, 163(2), 611–624. Available from: https://doi.org/10.1104/pp.113.225680

Choi, H.-S. & Cho, H.-T. (2019) Root hairs enhance Arabidopsis seedling survival upon soil disruption. *Scientific Reports*, 9(1), 11181. Available from: https://doi.org/10.1038/s41598-019-47733-0

Crombez, H., Motte, H. & Beeckman, T. (2019) Tackling plant phosphate starvation by the roots. *Developmental Cell*, 48(5), 599–615. Available from: https://doi.org/10.1016/j.devcel.2019.01.002

Curtis, M.D. & Grossniklaus, U. (2003) A gateway cloning vector set for high-throughput functional analysis of genes in planta. *Plant Physiology*, 133(2), 462–469. Available from: https://doi.org/10.1104/pp.103.027979

Czechowski, T., Stitt, M., Altmann, T., Udvardi, M.K. & Scheible, W.-R. (2005) Genome-wide identification and testing of superior reference genes for transcript normalization in *Arabidopsis*. *Plant Physiology*, 139(1), 5–17. Available from: https://doi.org/10.1104/pp.105.063743

Datta, S., Prescott, H. & Dolan, L. (2015) Intensity of a pulse of RSL4 transcription factor synthesis determines *Arabidopsis* root hair cell size. *Nat Plants*, 1, 15138. Available from: https://doi.org/10.1038/nplants.2015.138

Dietrich, P., Moeder, W. & Yoshioka, K. (2020) Plant cyclic nucleotide-gated channels: new insights on their functions and regulation. *Plant Physiology*, 184(1), 27–38. Available from: https://doi.org/10.1104/pp.20.00425

Feng, W., Kita, D., Peaucelle, A., Cartwright, H.N., Doan, V., Duan, Q. et al. (2018) The FERONIA receptor kinase maintains cell-wall integrity during salt stress through Ca^{2+} signaling. *Current Biology*, 28(5), 666–675. e665. Available from: https://doi.org/10.1016/j.cub.2018.01.023

Feng, Y., Xu, P., Li, B., Li, P., Wen, X., An, F. et al. (2017) Ethylene promotes root hair growth through coordinated EIN3/EIL1 and RHD6/RSL1 activity in *Arabidopsis*. *Proceedings of the National Academy of Sciences*, 114(52), 13834–13839. Available from: https://doi.org/10.1073/pnas.1711723115

Foreman, J., Demidchik, V., Bothwell, J.H., Mylona, P., Miedema, H., Torres, M.A. et al. (2003) Reactive oxygen species produced by NADPH oxidase regulate plant cell growth. *Nature*, 422(6930), 442–446. Available from: https://doi.org/10.1038/nature01485

Gao, Q.F., Gu, L.L., Wang, H.Q., Fei, C.F., Fang, X., Hussain, J. et al. (2016) Cyclic nucleotide-gated channel 18 is an essential Ca^{2+} channel in pollen tube tips for pollen tube guidance to ovules in *Arabidopsis*. *Proceedings of the National Academy of Sciences of the United States of America*, 113(11), 3096–3101. Available from: https://doi.org/10.1073/pnas.1524629113

Grierson, C., Nielsen, E., Ketelaarc, T. & Schiefelbein, J. (2014) Root hairs. *The Arabidopsis Book*, 12, e0172. Available from: https://doi.org/10.1199/tab.0172

Haling, R.E., Brown, L.K., Bengough, A.G., Young, I.M., Hallett, P.D., White, P.J. et al. (2013) Root hairs improve root penetration, root–soil contact, and phosphorus acquisition in soils of different strength. *Journal of Experimental Botany*, 64(12), 3711–3721. Available from: https://doi.org/10.1093/jxb/ert200

Hammond, J.P., Broadley, M.R. & White, P.J. (2004) Genetic responses to phosphorus deficiency. *Annali di Botanica*, 94(3), 323–332. Available from: https://doi.org/10.1093/aob/mch156

Han, X., Zhang, M., Yang, M. & Hu, Y. (2020) *Arabidopsis* JAZ proteins interact with and suppress RHD6 transcription factor to regulate jasmonate-stimulated root hair development. *The Plant Cell*, 32(4), 1049–1062. Available from: https://doi.org/10.1105/tpc.19.00617

Haring, M., Offermann, S., Danker, T., Horst, I., Peterhansel, C. & Stam, M. (2007) Chromatin immunoprecipitation: optimization, quantitative analysis and data normalization. *Plant Methods*, 3(1), 11. Available from: https://doi.org/10.1186/1746-4811-3-11

Hepler, P.K. (2005) Calcium: a central regulator of plant growth and development. *The Plant Cell*, 17(8), 2142–2155. Available from: https://doi.org/10.1105/tpc.105.032508

Himschoot, E., Beeckman, T., Friml, J. & Vanneste, S. (2015) Calcium is an organizer of cell polarity in plants. *Biochimica et Biophysica Acta/General Subjects*, 1853(9), 2168–2172. Available from: https://doi.org/10.1016/j.bbamcr.2015.02.017

Hwang, Y., Choi, H.-S., Cho, H.-M. & Cho, H.-T. (2017) Tracheophytes contain conserved orthologs of a basic helix–loop–helix transcription factor that modulate *ROOT HAIR SPECIFIC* genes. *The Plant Cell*, 29(1), 39–53. Available from: https://doi.org/10.1105/tpc.16.00732

Jain, A., Poling, M.D., Smith, A.P., Nagarajan, V.K., Lahner, B., Meagher, R.B. et al. (2009) Variations in the composition of gelling agents affect morphophysiological and molecular responses to deficiencies of phosphate and other nutrients. *Plant Physiology*, 150(2), 1033–1049. Available from: https://doi.org/10.1104/pp.109.136184

Jarratt-Barnham, E., Wang, L., Ning, Y. & Davies, J.M. (2021) The complex story of plant cyclic nucleotide-gated channels. *International Journal of Molecular Sciences*, 22(2), 874.

Jefferson, R.A., Kavanagh, T.A. & Bevan, M.W. (1987) GUS fusions: beta-glucuronidase as a sensitive and versatile gene fusion marker in higher plants. *The EMBO Journal*, 6(13), 3901–3907.

Kapulnik, Y., Delaux, P.M., Resnick, N., Mayzlish-Gati, E., Wininger, S., Bhattacharya, C. et al. (2011) Strigolactones affect lateral root formation and root-hair elongation in *Arabidopsis*. *Planta*, 233(1), 209–216. Available from: https://doi.org/10.1007/s00425-010-1310-y

Karimi, M., Inzé, D. & Depicker, A. (2002) GATEWAY™ vectors for *Agrobacterium*-mediated plant transformation. *Trends in Plant Science*, 7(5), 193–195. Available from: https://doi.org/10.1016/S1360-1385(02)02251-3

Kato, M., Aoyama, T. & Maeshima, M. (2013) The Ca^{2+}-binding protein PCaP2 located on the plasma membrane is involved in root hair development as a possible signal transducer. *The Plant Journal*, 74(4), 690–700. Available from: https://doi.org/10.1111/tpj.12155

Kim, C.M. & Dolan, L. (2016) ROOT HAIR DEFECTIVE SIX-LIKE Class I genes promote root hair development in the grass *Brachypodium distachyon*. *PLoS Genetics*, 12(8), e1006211. Available from: https://doi.org/10.1371/journal.pgen.1006211

Kim, C.M., Han, C.-d & Dolan, L. (2017) RSL class I genes positively regulate root hair development in *Oryza sativa*. *New Phytologist*, 213(1), 314–323. Available from: https://doi.org/10.1111/nph.14160

Konrad, K.R., Wudick, M.M. & Feijó, J.A. (2011) Calcium regulation of tip growth: new genes for old mechanisms. *Current Opinion in Plant Biology*, 14(6), 721–730. Available from: https://doi.org/10.1016/j.pbi.2011.09.005

Kudla, J. & Bock, R. (2016) Lighting the way to protein–protein interactions: recommendations on best practices for bimolecular fluorescence complementation analyses. *The Plant Cell*, 28(5), 1002–1008. Available from: https://doi.org/10.1105/tpc.16.00043

Kwon, T., Sparks, J.A., Liao, F. & Blancaflor, E.B. (2018) ERULUS is a plasma membrane-localized receptor-like kinase that specifies root hair growth by maintaining tip-focused cytoplasmic calcium oscillations. *The Plant Cell*, 30(6), 1173–1177. Available from: https://doi.org/10.1105/tpc.18.00316

Lynch, J.P. (2011) Root phenes for enhanced soil exploration and phosphorus acquisition: tools for future crops. *Plant Physiology*, 156(3), 1041–1049. Available from: https://doi.org/10.1104/pp.111.175414

Lynch, J.P. (2019) Root phenotypes for improved nutrient capture: an underexploited opportunity for global agriculture. *New Phytologist*, 223(2), 548–564. Available from: https://doi.org/10.1111/nph.15738

Ma, Z., Baskin, T.I., Brown, K.M. & Lynch, J.P. (2003) Regulation of root elongation under phosphorus stress involves changes in ethylene responsiveness. *Plant Physiology*, 131(3), 1381–1390. Available from: https://doi.org/10.1104/pp.012161

Mangano, S., Denita-Juarez, S.P., Choi, H.S., Marzol, E., Hwang, Y., Ranocha, P. et al. (2017) Molecular link between auxin and ROS-mediated polar growth. *Proceedings of the National Academy of Sciences of the United States of America*, 114(20), 5289–5294. Available from: https://doi.org/10.1073/pnas.1701536114

Mangano, S., Denita-Juarez, S.P., Marzol, E., Borassi, C. & Estevez, J.M. (2018) High auxin and high phosphate impact on RSL2 expression and ROS-homeostasis linked to root hair growth in *Arabidopsis thaliana*. *Frontiers in Plant Science*, 9(1164), Available from: https://doi.org/10.3389/fpls.2018.01164

Marin, M., Feeney, D.S., Brown, L.K., Naveed, M., Ruiz, S., Koebernick, N. et al. (2020) Significance of root hairs for plant performance under contrasting field conditions and water deficit. *Annals of Botany*, 128, 1–16. Available from: https://doi.org/10.1093/aob/mcaa181

Masucci, J.D. & Schiefelbein, J.W. (1994) The rhd6 mutation of *Arabidopsis thaliana* alters root-hair initiation through an auxin- and ethylene-associated process. *Plant Physiology*, 106(4), 1335–1346. Available from: https://doi.org/10.1104/pp.106.4.1335

Matthus, E., Wilkins, K.A., Swarbreck, S.M., Doddrell, N.H., Doccula, F.G., Costa, A. et al. (2019) Phosphate starvation alters abiotic-stress-induced cytosolic free calcium increases in roots. *Plant Physiology*, 179(4), 1754–1767. Available from: https://doi.org/10.1104/pp.18.01469

Monshausen, G.B., Messerli, M.A. & Gilroy, S. (2008) Imaging of the Yellow Cameleon 3.6 indicator reveals that elevations in cytosolic Ca^{2+} follow oscillating increases in growth in root hairs of *Arabidopsis*. *Plant Physiology*, 147(4), 1690–1698. Available from: https://doi.org/10.1104/pp.108.123638

Morcuende, R., Bari, R., Gibon, Y., Zheng, W., Pant, B.D., Bläsing, O. et al. (2007) Genome-wide reprogramming of metabolism and regulatory networks of *Arabidopsis* in response to phosphorus. *Plant, Cell & Environment*, 30(1), 85–112. Available from: https://doi.org/10.1111/j.1365-3040.2006.01608.x

Nelson, J.D., Denisenko, O. & Bomsztyk, K. (2006) Protocol for the fast chromatin immunoprecipitation (ChIP) method. *Nature Protocols*, 1(1), 179–185. Available from: https://doi.org/10.1038/nprot.2006.27

Nilsson, L., Muller, R. & Nielsen, T.H. (2007) Increased expression of the MYB-related transcription factor, PHR1, leads to enhanced phosphate uptake in *Arabidopsis thaliana*. *Plant, Cell & Environment*, 30(12), 1499–1512. Available from: https://doi.org/10.1111/j.1365-3040.2007.01734.x

Pan, Y., Chai, X., Gao, Q., Zhou, L., Zhang, S., Li, L. et al. (2019) Dynamic interactions of plant CNGC subunits and calmodulins drive oscillatory Ca^{2+} channel activities. *Developmental Cell*, 48(5), 710–725. e715. Available from: https://doi.org/10.1016/j.devcel.2018.12.025

Peng, J., Berbel, A., Madueño, F. & Chen, R. (2017) AUXIN RESPONSE FACTOR3 regulates compound leaf patterning by directly repressing PALMATE-LIKE PENTAFOLIATA1 expression in *Medicago truncatula*. *Frontiers of Plant Science*, 8, 1630. Available from: https://doi.org/10.3389/fpls.2017.01630

Pitts, R.J., Cernac, A. & Estelle, M. (1998) Auxin and ethylene promote root hair elongation in *Arabidopsis*. *The Plant Journal*, 16(5), 553–560. Available from: https://doi.org/10.1046/j.1365-313x.1998.00321.x

Plaxton, W.C. & Tran, H.T. (2011) Metabolic adaptations of phosphate-starved plants. *Plant Physiology*, 156(3), 1006–1015. Available from: https://doi.org/10.1104/pp.111.175281

Popescu, S.C., Popescu, G.V., Bachan, S., Zhang, Z., Seay, M., Gerstein, M. et al. (2007) Differential binding of calmodulin-related proteins to their targets revealed through high-density *Arabidopsis* protein microarrays. *Proceedings of the National Academy of Sciences*, 104(11), 4730–4735. Available from: https://doi.org/10.1073/pnas.0611615104

Raghothama, K.G. (1999) Phosphate acquisition. *Annual Review of Plant Physiology and Plant Molecular Biology*, 50(1), 665–693. Available from: https://doi.org/10.1146/annurev.arplant.50.1.665

Rincón-Zachary, M., Teaster, N.D., Sparks, J.A., Valster, A.H., Motes, C.M. & Blancaflor, E.B. (2010) Fluorescence resonance energy transfer-sensitized emission of yellow cameleon 3.60 reveals root zone-specific calcium signatures in *Arabidopsis* in response to aluminum and other trivalent cations. *Plant Physiology*, 152(3), 1442–1458. Available from: https://doi.org/10.1104/pp.109.147256

Rubio, V., Linhares, F., Solano, R., Martín, A.C., Iglesias, J., Leyva, A. et al. (2001) A conserved MYB transcription factor involved in phosphate starvation signaling both in vascular plants and in unicellular algae. *Genes and Development*, 15(16), 2122–2133. Available from: https://doi.org/10.1101/gad.204401

Saleh, A., Alvarez-Venegas, R. & Avramova, Z. (2008) An efficient chromatin immunoprecipitation (ChIP) protocol for studying histone modifications in *Arabidopsis* plants. *Nature Protocols*, 3(6), 1018–1025. Available from: https://doi.org/10.1038/nprot.2008.66

Schoenaers, S., Balcerowicz, D., Breen, G., Hill, K., Zdanio, M., Mouille, G. et al. (2018) The auxin-regulated CrRLK1L kinase ERULUS controls cell wall composition during root hair tip growth. *Current Biology*, 28(5), 722–732. e726. Available from: https://doi.org/10.1016/j.cub.2018.01.050

Song, L., Yu, H., Dong, J., Che, X., Jiao, Y. & Liu, D. (2016) The molecular mechanism of ethylene-mediated root hair development induced by phosphate starvation. *PLoS Genetics*, 12(7), e1006194. Available from: https://doi.org/10.1371/journal.pgen.1006194

Svistoonoff, S., Creff, A., Reymond, M., Sigoillot-Claude, C., Ricaud, L., Blanchet, A. et al. (2007) Root tip contact with low-phosphate media reprograms plant root architecture. *Nature Genetics*, 39(6), 792–796. Available from: https://doi.org/10.1038/ng2041

Tan, Y.-Q., Yang, Y., Zhang, A., Fei, C.-F., Gu, L.-L., Sun, S.-J. et al. (2020) Three CNGC family members, CNGC5, CNGC6, and CNGC9, are required for constitutive growth of *Arabidopsis* root hairs as Ca^{2+}-permeable channels. *Plant Communications*, 1(1), 100001. Available from: https://doi.org/10.1016/j.xplc.2019.100001

Thor, K. (2019) Calcium-nutrient and messenger. *Frontiers in Plant Science*, 10, 440. Available from: https://doi.org/10.3389/fpls.2019.00440

Tian, W., Wang, C., Gao, Q., Li, L. & Luan, S. (2020) Calcium spikes, waves and oscillations in plant development and biotic interactions. *Nature Plants*, 6(7), 750–759. Available from: https://doi.org/10.1038/s41477-020-0667-6

Tunc-Ozdemir, M., Rato, C., Brown, E., Rogers, S., Mooneyham, A., Frietsch, S. et al. (2013) Cyclic nucleotide gated channels 7 and 8 are essential for male reproductive fertility. *PLoS One*, 8(2), e55277. Available from: https://doi.org/10.1371/journal.pone.0055277

Vijayakumar, P., Datta, S. & Dolan, L. (2016) ROOT HAIR DEFECTIVE SIX-LIKE4 (RSL4) promotes root hair elongation by transcriptionally regulating the expression of genes required for cell growth. *The New Phytologist*, 212(4), 944–953. Available from: https://doi.org/10.1111/nph.14095

Vissenberg, K., Claeijs, N., Balcerowicz, D. & Schoenaers, S. (2020) Hormonal regulation of root hair growth and responses to the environment in *Arabidopsis*. *Journal of Experimental Botany*, 71(8), 2412–2427. Available from: https://doi.org/10.1093/jxb/eraa048

Waadt, R., Schlücking, K., Schroeder, J.I. & Kudla, J. (2014) Protein fragment bimolecular fluorescence complementation analyses for the in vivo study of protein–protein interactions and cellular protein complex localizations. In: Sanchez-Serrano, J.J. & Salinas, J. (Eds.) *Arabidopsis protocols*. Totowa, NJ: Humana Press, pp. 629–658.

Wang, T., Li, C., Wu, Z., Jia, Y., Wang, H., Sun, S. et al. (2017) Abscisic acid regulates auxin homeostasis in rice root tips to promote root hair

elongation. *Frontiers in Plant Science*, 8(1121), 1121. Available from: https://doi.org/10.3389/fpls.2017.01121

Williamson, L.C., Ribrioux, S.P.C.P., Fitter, A.H. & Leyser, H.M.O. (2001) Phosphate availability regulates root system architecture in *Arabidopsis*. *Plant Physiology*, 126(2), 875–882. Available from: https://doi.org/10.1104/pp.126.2.875

Won, S.-K., Lee, Y.-J., Lee, H.-Y., Heo, Y.-K., Cho, M. & Cho, H.-T. (2009) *cis*-Element- and transcriptome-based screening of root hair-specific genes and their functional characterization in *Arabidopsis*. *Plant Physiology*, 150(3), 1459–1473. Available from: https://doi.org/10.1104/pp.109.140905

Yi, K., Menand, B., Bell, E. & Dolan, L. (2010) A basic helix–loop–helix transcription factor controls cell growth and size in root hairs. *Nature Genetics*, 42(3), 264–267. Available from: https://doi.org/10.1038/ng.529

Ying, S. (2021) Genome-wide identification and transcriptional analysis of *Arabidopsis* DUF506 gene family. *International Journal of Molecular Sciences*, 22(21), 11442. Available from: https://doi.org/10.3390/ijms222111442

Ying, S., Blancaflor, E.B., Liao, F. & Scheible, W.-R. (2022) A phosphorus-limitation induced, functionally conserved DUF506 protein is a repressor of root hair elongation in plants. *New Phytologist*, 233(3), 1153–1171. Available from: https://doi.org/10.1111/nph.17862

Yu, X., Xu, G., Li, B., de Souza Vespoli, L., Liu, H., Moeder, W. et al. (2019) The receptor kinases BAK1/SERK4 regulate Ca^{2+} channel-mediated cellular homeostasis for cell death containment. *Current Biology*, 29(22), 3778–3790. e3778. Available from: https://doi.org/10.1016/j.cub.2019.09.018

Yuan, P., Jauregui, E., Du, L., Tanaka, K. & Poovaiah, B.W. (2017) Calcium signatures and signaling events orchestrate plant–microbe interactions. *Current Opinion in Plant Biology*, 38, 173–183. Available from: https://doi.org/10.1016/j.pbi.2017.06.003

Zeb, Q., Wang, X., Hou, C., Zhang, X., Dong, M., Zhang, S. et al. (2020) The interaction of CaM7 and CNGC14 regulates root hair growth in *Arabidopsis*. *Journal of Integrative Plant Biology*, 62(7), 887–896. Available from: https://doi.org/10.1111/jipb.12890

Zhang, S., Pan, Y., Tian, W., Dong, M., Zhu, H., Luan, S. et al. (2017) Arabidopsis CNGC14 mediates calcium influx required for tip growth in root hairs. *Molecular Plant*, 10(7), 1004–1006. Available from: https://doi.org/10.1016/j.molp.2017.02.007

Zhang, X., Henriques, R., Lin, S.S., Niu, Q.W. & Chua, N.H. (2006) *Agrobacterium*-mediated transformation of *Arabidopsis thaliana* using the floral dip method. *Nature Protocols*, 1(2), 641–646. Available from: https://doi.org/10.1038/nprot.2006.97

Zhang, X., Mi, Y., Mao, H., Liu, S., Chen, L. & Qin, F. (2020) Genetic variation in ZmTIP1 contributes to root hair elongation and drought tolerance in maize. *Plant Biotechnology Journal*, 18(5), 1271–1283. Available from: https://doi.org/10.1111/pbi.13290

Zhu, S., Martínez Pacheco, J., Estevez, J.M. & Yu, F. (2020) Autocrine regulation of root hair size by the RALF-FERONIA-RSL4 signaling pathway. *New Phytologist*, 227(1), 45–49. Available from: https://doi.org/10.1111/nph.16497

Zielinski, R.E. (1998) Calmodulin and calmodulin-binding proteins in plants. *Annual Review of Plant Physiology and Plant Molecular Biology*, 49, 697–725. Available from: https://doi.org/10.1146/annurev.arplant.49.1.697

SUPPORTING INFORMATION

Additional supporting information may be found in the online version of the article at the publisher's website.

How to cite this article: Ying, S. & Scheible, W.-R. (2022) A novel calmodulin-interacting Domain of Unknown Function 506 protein represses root hair elongation in *Arabidopsis*. *Plant, Cell & Environment*, 45, 1796–1812. https://doi.org/10.1111/pce.14316